NASA
Technical
Paper
2214

January 1984

An Analysis of Shock Coalescence Including Three-Dimensional Effects With Application to Sonic Boom Extrapolation

Christine M. Darden

NASA

NASA
Technical
Paper
2214

1984

An Analysis of Shock Coalescence Including Three-Dimensional Effects With Application to Sonic Boom Extrapolation

Christine M. Darden

Langley Research Center
Hampton, Virginia

NASA
National Aeronautics
and Space Administration

**Scientific and Technical
Information Office**

1984

CONTENTS

SUMMARY v

SYMBOLS vii

1. INTRODUCTION 1
   1.1 Purpose 1
   1.2 Review of Sonic Boom Work 1
   1.3 Outline of Discussion 3

2. THEORETICAL BACKGROUND FOR MMOC SONIC BOOM PROPAGATION METHOD 4
   2.1 Governing Equations and Closure Conditions 4
   2.2 Shock Conditions 10
   2.3 Method of Solution 10
   2.4 Far-Field Modifications 11

3. COALESCENCE OF SHOCKS 12
   3.1 Axisymmetric Shock Coalescence 12
      3.1.1 Governing equations 12
      3.1.2 Method of solution 14
   3.2 Asymmetric Shock Coalescence 16
      3.2.1 Derivation of shock equations 16
      3.2.2 Asymmetric analysis 19
      3.2.3 Asymmetric solution process 24

4. SPATIAL DERIVATIVES NEEDED FOR ASYMMETRIC SOLUTION 29
   4.1 Spatial Derivatives in Regions 4 and 5 29
   4.2 Spatial Derivatives in Regions 1 and 3 33

5. PROCEDURE FOR COMBINING COALESCENCE WITH MMOC PROGRAM 35
   5.1 Establishing Point of Coalescence 35
   5.2 Local Solution 38
   5.3 Incorporation of Solution into Characteristic Network 38

6. RESULTS AND DISCUSSION 40

7. CONCLUDING REMARKS 43

REFERENCES 45

SUMMARY

A method for analyzing shock coalescence which includes three-dimensional effects is developed. This method is based on an extension of the axisymmetric solution. The asymmetric effects are introduced through an additional set of governing equations, which are derived by taking the second circumferential derivative of the standard shock equations in the plane of symmetry. The coalescence method is consistent with and has been combined with a nonlinear sonic boom extrapolation program which is based on the method of characteristics. Though the two sets of governing shock equations are uncoupled, the flow equations, developed in the same manner, are weakly coupled through the first derivative of the circumferential velocity. Since the characteristic behind the shock is necessary to fix shock location, an iterative procedure between the axisymmetric and asymmetric equations is used. The extrapolation program, originally unable to handle shock coalescence, is now able to extrapolate pressure signatures which include embedded shocks from an initial data line in the plane of symmetry at approximately one body length from the axis of the aircraft to the ground.

Descriptions of the axisymmetric shock coalescence solution, the asymmetric shock coalescence solution, the method of incorporating these solutions into the extrapolation program, and the methods used to determine spatial derivatives needed in the coalescence solution are included. Results of the method are shown for a body of revolution at a small, positive angle of attack. The body was designed so that embedded shocks would be included in the near-field data. These results are compared with results from two widely used sonic boom propagation methods which are based on modified linear theory. Signatures are shown at several stages of the extrapolation process through the atmosphere in an attempt to understand the reasons for the differences in the results of the three methods.

SYMBOLS

A	dummy variable used to derive equation (3.32)
A_c	constant of integration
a	speed of sound
B_1-B_5	variables used to define equations (3.58) and (3.59)
C^-, C^+	characteristics
$C^{-'}$	intermediate characteristic calculated at intersection point
C_p	pressure coefficient
c_p	specific heat at constant pressure
d	$= Y - z$
E	defined below equation (2.33)
F	$= r^{1/2} \dfrac{\nabla p}{p}$
$\mathcal{J}$	defined below equation (2.30)
f	shock surface, $x = f(r,\phi)$
$\bar{f}$	shock in plane $\phi = 0$, $x = f(r,0)$
$\tilde{f}$	$= \left.\dfrac{\partial^2 f}{\partial \phi^2}\right\vert_{\phi=0}$
$\vec{G}$	body force vector per unit mass
g	acceleration due to gravity
$\bar{g}$	acceleration due to gravity in plane of symmetry
H	enthalpy, $H(x,r,\phi)$
$\bar{H}$	enthalpy in plane $\phi = 0$, $H(x,r,0)$
$\tilde{H}$	$= \left.\dfrac{\partial^2 H}{\partial \phi^2}\right\vert_{\phi=0}$
h	slipstream surface, $r = h(x,\phi)$
$\bar{h}$	slipstream in plane $\phi = 0$, $r = h(x,0)$
$\tilde{h}$	$= \left.\dfrac{\partial^2 h}{\partial \phi^2}\right\vert_{\phi=0}$

I	index used for counting C^- characteristics
ϑ_1, ϑ_2	variables used to define equation (3.60)
$\hat{i}$	unit vector in x direction
J	right side of equation (2.25)
$\hat{j}$	unit vector in r direction
k_∞	$= \frac{\gamma + 1}{\gamma} \frac{M_\infty^2}{\beta_\infty}$
L_1, L_2, L_3	variables used to define equations (3.58) and (3.59)
ℓ	length used to nondimensionalize x, r, and d
M	Mach number
m	mass
N	counter used in iterations
n	direction normal to streamline
$\hat{n}$	unit vector in normal direction
p	pressure
$\bar{p}$	$= p(x,r,0)$
$\tilde{p}$	$= \left.\frac{\partial^2 p}{\partial \psi^2}\right\|_{\psi=0}$
Q	defined below equation (3.31)
$\bar{Q}$	defined below equation (3.34)
$\tilde{Q}$	defined below equation (3.34)
q	$= \|\vec{v}\|$
$\bar{q}$	$= \sqrt{\bar{u}^2 + \bar{v}^2}$
R	gas constant
$\tilde{R}$	$= \left.\frac{\partial^2 R(\psi)}{\partial \psi^2}\right\|_{\psi=0}$
Ra	notation used in sketch F

Rb	notation used in sketch F
Re	r coordinate of shock intersection
Re'	previous r coordinate of intersection location in iterations
$R(\psi)$	r coordinate of surface intersections, $r = R(\psi)$
r	radial coordinate
S	entropy
$\bar{S}$	$= S(x,r,0)$
$\tilde{S}$	$= \left.\frac{\partial^2 S}{\partial \psi^2}\right\|_{\psi=0}$
ΔS_{sh}	jump in entropy across shock
T	temperature
$\bar{T}$	$= \frac{RT}{u_\infty^2}$ in plane $\psi = 0$
$\tilde{T}$	$= \left.\frac{\partial^2 T}{\partial \psi^2}\right\|_{\psi=0}$
U	velocity
u	axial component of velocity
$\bar{u}$	$= \frac{u(x,r)\big\|_{\psi=0}}{U_\infty}$
$\tilde{u}$	$= \frac{\left.\frac{\partial^2 u}{\partial \psi^2}\right\|_{\psi=0}}{U_\infty}$
ua	axial velocity at Ra in sketch F
ub	axial velocity at Rb in sketch F
$\vec{V}$	velocity vector
v	radial component of velocity
$\bar{v}$	$= \frac{v(x,r)\big\|_{\psi=0}}{U_\infty}$

$\tilde{v}$ $= \dfrac{\left.\dfrac{\partial^2 v}{\partial \psi^2}\right|_{\psi=0}}{U_\infty}$

va radial velocity at Ra in sketch F

vb radial velocity at Rb in sketch F

w circumferential component of velocity

$\hat{w}$ $= \dfrac{\left.\dfrac{\partial w}{\partial \psi}\right|_{\psi=0}}{U_\infty}$

X x intersection of five surfaces, $x = X(\psi)$, see sketch D

$\tilde{X}$ $= \left.\dfrac{\partial^2 X}{\partial \psi^2}\right|_{\psi=0}$

Xe x coordinate of shock intersection in plane $\psi = 0$

Xe' previous x coordinate of intersection point in iteration

XI shock intersection with C^- characteristic (see sketch J)

Xp x coordinate of resultant shock intersection with next C^- characteristic (see sketch L)

x axial coordinate

x_o starting location of pressure signature

Y flight altitude

y vertical coordinate

z distance of calculation point from ground

α angle of attack

β shock angle, $\sqrt{M^2 - 1}$

β' previous value of shock angle used in iteration

γ ratio of specific heats

ε error criteria

θ flow angle

$\bar{\theta}$ flow angle in plane $\psi = 0$

μ Mach angle, $\sin^{-1}\left(\frac{1}{M}\right)$

ν	Prandtl-Meyer angle
ρ	density
σ	distance along streamline
ϕ	coordinate in circumferential direction
$\hat{\phi}$	unit vector in circumferential direction
∇	del, $\hat{i}\,\frac{\partial}{\partial x} + \hat{j}\,\frac{\partial}{\partial r} + \frac{\hat{\phi}}{r}\,\frac{\partial}{\partial \phi}$

Subscripts:

n	normal component
r	$\frac{\partial}{\partial r}$
rr	$\frac{\partial^2}{\partial r^2}$
rx	$\frac{\partial^2}{\partial r\ \partial x}$
$r\phi$	$\frac{\partial^2}{\partial r\ \partial \phi}$
$r\phi\phi$	$\frac{\partial^3}{\partial r\ \partial \phi^2}$
T	total conditions
t	tangential component
x	$\frac{\partial}{\partial x}$
xx	$\frac{\partial^2}{\partial x^2}$
$x\phi$	$\frac{\partial^2}{\partial x\ \partial \phi}$
ϕ	$\frac{\partial}{\partial \phi}$
$\phi\phi$	$\frac{\partial^2}{\partial \phi^2}$
∞	free-stream conditions
1,2,3,4	shock surfaces

1,2,3,4,5	regions in intersection problem

Notation over symbols:

→	denotes a vector
^	denotes a unit vector
-	denotes a variable evaluated in the vertical plane $\phi = 0$
~	denotes the second partial derivative of a variable with respect to ϕ evaluated in the vertical plane $\phi = 0$

Abbreviations:

ARAP	sonic boom extrapolation method developed by Aeronautical Research Associates of Princeton
alt	altitude
MMOC	modified method of characteristics
MUAM	modified uniform atmosphere method

1. INTRODUCTION

1.1 Purpose

This paper presents an analysis and method of solution for shock coalescence with asymmetric effects. The analysis is consistent with and an extension of a sonic boom propagation theory developed at New York University (refs. 1 to 3) and has been incorporated into the computer program associated with that work. To provide information on the need for and the importance of this work, a brief review of sonic boom prediction, extrapolation, minimization, test methods, and some weaknesses of these methods is included in the next section.

1.2 Review of Sonic Boom Work

The sonic boom continues to be a major obstacle in the path of the development of an economically viable supersonic transport fleet. Though much progress has been made in understanding, predicting, and minimizing the sonic boom, the ultimate goal of producing an aircraft with sonic boom characteristics acceptable for overland flight remains elusive.

Most currently used prediction methods are based on theories developed by Whitham (ref. 4) for a supersonic projectile, and by Walkden (ref. 5), who extended the analysis to include lifting bodies. These theories combined with the supersonic area rule theory developed by Hayes (ref. 6) led to the generally accepted prediction methods described in some detail in reference 7. Originally, it was felt that all sonic boom pressure signatures would have attained the standard N-wave shape when they intersected the ground. Work by McLean (ref. 8) indicated that for airplanes with extensive lifting surfaces this was not so. The "freezing" effects of the real atmosphere pointed out by Hayes (ref. 9) reinforced the idea that the signature may still retain midfield effects when it intersects the ground. A midfield signature retains effects of the airplane shape and thus offers this shaping as a possible avenue of minimizing the sonic boom.

Using as a basis the sonic boom prediction method, the idea of a midfield signature, and work by Jones (ref. 10) on the far-field minimum, Seebass and George developed a minimization procedure (refs. 11 and 12) which predicted a minimizing equivalent area distribution for given flight conditions. Extensions to this procedure for the real atmosphere and nose bluntness relaxation are given in references 13 and 14. Working inversely, the designer can develop a model whose area matches the above boom-constrained distribution. This process was used in the design of three wing-body configurations, which were tested experimentally for sonic boom levels (refs. 15 and 16). Conclusions from that study indicated that the approach is valid, but that the boundary layer and wake effects must be considered in the design process. Two feasibility studies (refs. 17 and 18), in which systems, passenger loads, safety, and efficiency considerations were included, indicated that a low-boom aircraft was within the realm of possibility, but that extensive in-depth studies and trade-offs were needed. Certain characteristic features of low-boom aircraft seemed to evolve from the studies. These features included a large wing area, long root chord, positive dihedral, twist, camber, and canards.

As theoretical sonic boom studies have evolved, so have the accompanying test methods. The earliest propagation methods were based entirely on far-field theory and thus required as input data a far-field N wave. In order for the pressure signature to have traveled a sufficient number of body lengths to have attained its N wave form in the existing supersonic tunnels, model size was limited to approximately 1 inch. With the advance in knowledge of the importance of the midfield signature and the development of propagation methods which accepted this data, wind-tunnel model size became limited by the requirement that the data be axisymmetric. Since tests have shown that disturbances caused by volume are nearly axisymmetric at about three body lengths away and that those caused by the lifting forces have also lost much of their asymmetry, this lowered restraint generally allowed model size to increase to approximately 6 inches. Model builders can include many more features in a 6-inch model than in one which is only 1 inch. Even so, details such as twist, camber, and nacelles are still nearly impossible to include on a 1/50-scale model with the accuracy needed.

To increase the reliability of testing the latest low-boom transport designs, the models should be limited only by tunnel size and flow quality within the tunnel. This would allow model size to increase to roughly 2 feet in span and 3 feet in length. This size would allow one model to be used for both force and sonic boom tests. In addition to allowing improved accuracy in construction, this size also reduces the problems with the boundary layer and the sting support system (ref. 19).

Propagation methods based on linearized theory become inaccurate for strong shocks where significant entropy changes occur and for high altitude and Mach numbers where the cumulative effects of second-order terms become significant (ref. 20). The propagation method (refs. 1 and 2) developed at New York University (NYU) by Ferri, Siclari, and Ting eliminates many of these problems. Nonlinear terms have been retained, and altitude effects and entropy effects are included. The method of solution is the modified method of characteristics (MMOC), in which step sizes on the order of several body lengths may be taken without destroying the accuracy of the program. The program includes nonlinear effects, which are important in the near field, but still does not account for nonaxisymmetric effects, which are also very prominent. A second program (ref. 3), developed by Ferri, Ting, and Lo, includes the asymmetric effects near the vertical line of symmetry - where sonic boom effects are strongest. This is accomplished by bringing in three-dimensional effects through derivatives in the circumferential direction which do not vanish in the vertical plane of symmetry. The method introduces the effects of asymmetry without the prohibitive difficulty of the full three-dimensional method of characteristics.

As stated, the low-boom transport model will have a very complicated, rotational near field with embedded shocks from the wing-fuselage juncture, from engine pods, and from other parts of the aircraft. In the near field, these embedded shocks will not have coalesced into one shock. Though the NYU program accepts input at approximately one body length, it cannot handle the coalescence of shocks, and thus, calculations cease.

Using the same approach as that used to include the three-dimensional effects in the MMOC program, this paper presents the analysis for axisymmetric and nonaxisymmetric shock coalescence.

1.3 Outline of Discussion

As previously stated, the major contribution of this paper is the analysis and solution for shock coalescence with asymmetric effects, as described in section 3. However, because this method was developed to be used with the MMOC program, it is also necessary to describe in some detail the methods of that program, the method in which the shock coalescence is combined with the MMOC program, and the methods used to find additional information needed for the solution.

To this end, a fairly detailed description of the equations and method of solution of the MMOC program are given in section 2. Also included in that section is a description of the closure condition of the method. The limitations introduced into the outgoing characteristic to enable larger step sizes are also described.

Section 3 includes the analysis and method of solution for shock coalescence - both the axisymmetric and asymmetric cases. Once the point of shock intersection is located, the axisymmetric solution is found and then the asymmetric solution. No iteration is needed, since the axisymmetric and asymmetric governing equations are not coupled.

Spatial derivatives such as u_x and u_r are necessary for the asymmetric coalescence solution, and these variables are not defined in the MMOC program. Section 4 describes the methods used to obtain their values. Used in section 4 is a method developed by Lin and Rubinov (ref. 21), which states that if the curvature of a shock is known, then the spatial derivatives behind the shock are also known. The system of equations for the derivatives becomes indeterminate for shocks of zero strength and, therefore, unsuitable for numerical computations with weak shocks. In the current analysis, it is assumed that the resultant shock is of finite strength, but the isentropic shock or expansion wave of the opposite family needed to equalize the system is so weak that continuity of the variables across the wave may be used. For shocks of zero strength, the curvature of the shock (or that of the centerline of an expansion fan) differs from that of the characteristic ahead of and behind the shock because of the jump of the curvature of the streamline, which is continuous in slope. To generalize the system for shocks of any strength, it is necessary to regroup the equations in such a way that the common factor which vanishes for zero shock strength cancels analytically.

The procedure for combining the shock coalescence with the MMOC program is described in section 5. This section includes a description of how the intersection point is found, how data immediately in front of the intersection point are determined, the solution, and then how the solution is recombined with the characteristic network.

Section 6 describes results which were obtained for a lifting body of revolution with embedded shock coalescence during propagation. It is beyond the scope of this paper to conduct a parametric study with many different bodies. Rather, the emphasis is placed on the development and incorporation of the method of shock coalescence with the MMOC program, and a simple body of revolution is used to illustrate the results. Extrapolated data from the MMOC program are compared with results from two well-known sonic boom prediction methods which are based on modified linear theory.

This work was done to satisfy in part the requirements for the degree of Doctor of Science at George Washington University, February 1983.

2. THEORETICAL BACKGROUND FOR MMOC SONIC BOOM PROPAGATION METHOD

2.1 Governing Equations and Closure Conditions

The analysis developed in this paper is an extension of the methods developed in references 1 to 3. Governing equations for the steady-state, inviscid flow field including gravitational terms and variation in total energy are (ref. 22)

Momentum

$$\vec{V} \cdot \nabla\vec{V} = -\frac{\nabla p}{\rho} + \vec{G} \tag{2.1}$$

Continuity

$$\rho\nabla \cdot \vec{V} + \vec{V} \cdot \nabla\rho = 0 \tag{2.2}$$

Energy

$$\vec{V} \cdot \nabla H = 0 \tag{2.3}$$

State

$$p = \rho RT \tag{2.4}$$

where the total enthalpy H is defined by

$$H = \frac{\gamma}{\gamma - 1} RT + \frac{q^2}{2} + gz \tag{2.5}$$

In these equations, g is the acceleration due to gravity, $\vec{G}$ is the body force vector per unit mass $\left(\vec{G} = -g\,\nabla z,\right.$ where z is the vertical coordinate$\left.\right)$, R is the gas constant, and q is the fluid speed $\left(q = |\vec{V}|\right)$.

It is convenient for computational purposes to transform the set of governing equations. The Gibbs relation (ref. 23) is introduced in the form

$$T\,\nabla S = \frac{\gamma R}{\gamma - 1} \nabla T - \frac{1}{\rho} \nabla p \tag{2.6}$$

where S is the fluid entropy per unit mass. Use of equation (2.6) and the relation $\vec{V} \cdot \nabla\vec{V} = \nabla\left(q^2/2\right) + \left(\nabla \times \vec{V}\right) \times \vec{V}$ allows pressure and density to be eliminated from the momentum and continuity equations, which become

$$\left(\nabla \times \vec{V}\right) \times \vec{V} = T\,\nabla S - \nabla H \tag{2.7}$$

and

$$\nabla \cdot \vec{V} = \frac{\vec{V}}{a^2} \cdot \nabla\left(\frac{q^2}{2}\right) - \frac{\vec{V} \cdot \vec{G}}{a^2} \tag{2.8}$$

in which the speed of sound a is given by $a^2 = \gamma RT$. It is noted here for later use that in view of equation (2.3), the component of equation (2.7) along a streamline is

$$\vec{V} \cdot \nabla S = 0 \tag{2.9}$$

Ahead of the bow shock, the flow is assumed to be uniform with velocity U_∞. The temperature $T_\infty(z)$ and the pressure $p_\infty(z)$ are given functions of the altitude z which satisfy the condition of hydrostatic equilibrium

$$\frac{T_\infty(z)}{p_\infty(z)} \frac{dp_\infty(z)}{dz} = -\frac{g}{R}$$

Jump conditions for the system consisting of equations (2.3) to (2.8) are discussed in detail later. However, it is pointed out here that the total enthalpy remains constant across a stationary shock wave (ref. 23). This, together with equation (2.3) implies that H is invariant along streamlines

$$H = \frac{\gamma}{\gamma - 1} RT + \frac{q^2}{2} + gz = \frac{\gamma}{\gamma - 1} RT_\infty(z_\infty) + \frac{U_\infty^2}{2} + gz_\infty \tag{2.10}$$

where the notation z_∞ is introduced to denote the elevation of a particular streamline in the uniform flow ahead of the bow shock. In the numerical computations described later, the function $z_\infty(x,y,z)$ was actually calculated instead of H itself, by replacing equation (2.3) with $\vec{V} \cdot \nabla z_\infty = 0$. Once z_∞ or H and the velocity are known, then T can be considered as known from equation (2.10). Thus, the system consisting of equations (2.3), (2.7), and (2.8) can be regarded as a system of five equations for five unknowns: u, v, w, S, and H.

For an airplane flying at constant altitude Y, it is convenient to introduce cylindrical coordinates x, r, ϕ, shown in sketch A, with velocity components u, v, w where

$$z = Y - r \cos \phi$$

and

$$\nabla = \hat{i} \frac{\partial}{\partial x} + \hat{j} \frac{\partial}{\partial r} + \frac{\hat{\phi}}{r} \frac{\partial}{\partial \phi}$$

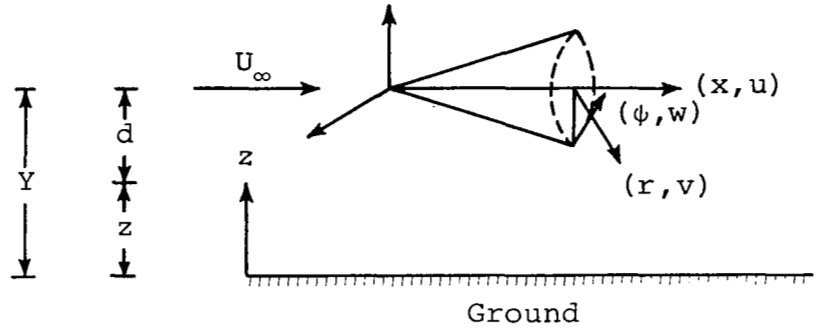

Sketch A

In this coordinate system, the five fundamental equations (2.3), (2.7), and (2.8) are expressed as

$$u \frac{\partial H}{\partial x} + v \frac{\partial H}{\partial r} + \frac{w}{r} \frac{\partial H}{\partial \phi} = 0 \tag{2.11}$$

$$\frac{\partial u}{\partial x} + \frac{\partial v}{\partial r} + \frac{v}{r} + \frac{1}{r} \frac{\partial w}{\partial \phi} = \frac{1}{a^2}\left(u \frac{\partial}{\partial x} + v \frac{\partial}{\partial r} + \frac{w}{r} \frac{\partial}{\partial \phi}\right)\left(\frac{u^2 + v^2 + w^2}{2} + gz\right) \tag{2.12}$$

$$T \frac{\partial S}{\partial x} - \frac{\partial H}{\partial x} = v\left(\frac{\partial u}{\partial r} - \frac{\partial v}{\partial x}\right) + w\left(\frac{1}{r} \frac{\partial u}{\partial \phi} - \frac{\partial w}{\partial x}\right) \tag{2.13}$$

$$T \frac{\partial S}{\partial r} - \frac{\partial H}{\partial r} = u\left(\frac{\partial v}{\partial x} - \frac{\partial u}{\partial r}\right) + w\left(\frac{1}{r} \frac{\partial v}{\partial \phi} - \frac{\partial w}{\partial r} - \frac{w}{r}\right) \tag{2.14}$$

$$\frac{T}{r} \frac{\partial S}{\partial \phi} - \frac{1}{r} \frac{\partial H}{\partial \phi} = u\left(\frac{\partial w}{\partial x} - \frac{1}{r} \frac{\partial u}{\partial \phi}\right) + v\left(\frac{\partial w}{\partial r} - \frac{1}{r} \frac{\partial v}{\partial \phi} + \frac{w}{r}\right) \tag{2.15}$$

In the vertical plane of symmetry, the circumferential velocity w vanishes as do the first derivatives of all variables except w with respect to the circumferential direction. Thus in the plane $\phi = 0$, equations (2.11) to (2.14) become

$$u \frac{\partial H}{\partial x} + v \frac{\partial H}{\partial r} = 0 \tag{2.16}$$

$$\left(1 - \frac{u^2}{a^2}\right) \frac{\partial u}{\partial x} + \left(1 - \frac{v^2}{a^2}\right) \frac{\partial v}{\partial r} - \frac{uv}{a^2}\left(\frac{\partial u}{\partial r} + \frac{\partial v}{\partial x}\right) + \frac{v}{r} + \frac{1}{r} \frac{\partial w}{\partial \phi} + \frac{gv}{a^2} = 0 \tag{2.17}$$

$$T \frac{\partial S}{\partial x} - \frac{\partial H}{\partial x} = v\left(\frac{\partial u}{\partial r} - \frac{\partial v}{\partial x}\right) \tag{2.18}$$

$$T\frac{\partial S}{\partial r} - \frac{\partial H}{\partial r} = u\left(\frac{\partial v}{\partial x} - \frac{\partial u}{\partial r}\right) \tag{2.19}$$

Equation (2.15) is identically satisfied in the plane $\psi = 0$.

Equations (2.18) and (2.19) are combined to give

$$\frac{\partial v}{\partial x} - \frac{\partial u}{\partial r} = \frac{1}{q}\left(T\frac{\partial S}{\partial n} - \frac{\partial H}{\partial n}\right) \tag{2.20}$$

where $q\,\partial/\partial n = u(\partial/\partial r) - v(\partial/\partial x)$, and $\partial/\partial n$ is the derivative normal to the streamline. Equation (2.20) represents one scalar component of the original vector equation (2.7). The second independent relation will be taken to be equation (2.9), which in the plane of symmetry becomes

$$u\frac{\partial S}{\partial x} + v\frac{\partial S}{\partial r} = 0 \tag{2.21}$$

Equations (2.16), (2.17), (2.20), and (2.21) now form a set of four equations with five unknowns: u, v, S, H, and $\partial w/\partial\psi$. For the axisymmetric approximation, it is assumed that the term $(1/r)(\partial w/\partial\psi)$ is negligible at large values of r. Thus, a closed system of equations is attained. If this assumption is not made, then another method for closing the system must be found.

Since equation (2.15) is an identity in the plane $\psi = 0$, its first derivative with respect to ψ is taken. This process introduces an additional equation, but it also introduces several new unknowns. The second derivative with respect to ψ is taken of equations (2.11) to (2.14) and (2.9). The derivatives of equations (2.13) and (2.14) are combined by multiplying (2.13) by u/q and subtracting the product of v/q and equation (2.14). This process introduces five new equations and five new unknowns: $\partial^2u/\partial\psi^2$, $\partial^2v/\partial\psi^2$, $\partial^2H/\partial\psi^2$, $\partial^2S/\partial\psi^2$, and $\partial^3w/\partial\psi^3$. The entire system now consists of 9 equations and 10 unknowns.

The closure assumption introduced in references 1 to 3 is

$$\frac{\partial^3 w}{\partial\psi^3} \approx -\frac{\partial w}{\partial\psi} \tag{2.22}$$

This assumption is justified on the basis that the primary contribution to the cross flow can be described by a function of the form

$$w \sim w(x,r)\sin\psi$$

which is a valid approximation describing asymmetries due to lift or small asymmetries which are present at approximately one to two body lengths from an aircraft. With the closure condition, the system reduces to nine equations and nine unknowns.

The last five equations formed by taking derivatives in the circumferential direction are listed below where the closure condition, equation (2.22), has already been applied. For convenience, the following notation is introduced:

$$\bar{u} = \frac{u(x,r)\big|_{\psi=0}}{U_\infty} \qquad \bar{u}_x = \frac{\frac{\partial u}{\partial x}\Big|_{\psi=0}}{U_\infty} \qquad \tilde{u} = \frac{\frac{\partial^2 u}{\partial \psi^2}\Big|_{\psi=0}}{U_\infty} \qquad \hat{w} = \frac{\frac{\partial w}{\partial \psi}\Big|_{\psi=0}}{U_\infty}$$

Equations (2.11) to (2.15) yield

$$\tilde{u}\bar{H}_x + \bar{u}\tilde{H}_x + \tilde{v}\bar{H}_r + \bar{v}\tilde{H}_r + \frac{2\hat{w}}{r}\tilde{H} = 0 \tag{2.23}$$

$$\begin{aligned}\tilde{u}_x + \tilde{v}_r - \frac{1}{\bar{a}^2}\left[\bar{u}^2\tilde{u}_x + \bar{u}\bar{v}\left(\tilde{u}_r + \tilde{v}_x\right) + \bar{v}^2\tilde{v}_r\right] = \frac{\tilde{v}}{r} + \frac{\hat{w}}{r} + \frac{1}{\bar{a}^2}\Bigg[&\tilde{u}\left(2\bar{u}\bar{u}_x + \bar{v}\bar{u}_r + \bar{v}\bar{v}_x\right)\\ &+ \tilde{v}\left(2\bar{v}\bar{v}_r + \bar{u}\bar{v}_x + \bar{u}\bar{u}_r\right) + g\left(\bar{v} - \tilde{v}\right)\\ &+ 2\hat{w}\left(\bar{v}\hat{w}_r + \bar{u}\hat{w}_x + \bar{g}\right) + \frac{2\hat{w}}{r}\left(\bar{v}\tilde{v} + \bar{u}\tilde{u}\right.\\ &\left. + \hat{w}^2\right) - \tilde{a}^2\left(\bar{u}_x + \frac{\bar{v}}{r} + \bar{v}_r + \frac{\hat{w}}{r}\right)\Bigg]\end{aligned} \tag{2.24}$$

$$\begin{aligned}\tilde{u}_r - \tilde{v}_x = \frac{1}{q}\Bigg[&\frac{\partial H}{\partial n} - \bar{T}\frac{\partial S}{\partial n} - \tilde{T}\frac{d\bar{S}}{dn} + \frac{1}{q^2}\left(\bar{u}\tilde{u} + \bar{v}\tilde{v}\right)\left(\bar{T}\frac{dS}{dn} - \frac{dH}{dn}\right)\\ &+ \frac{2\hat{w}}{q}\left(\frac{\bar{u}\tilde{v} - \bar{v}\tilde{u} - \bar{u}\hat{w}}{r} - q\frac{\partial \hat{w}}{\partial n}\right)\Bigg]\end{aligned} \tag{2.25}$$

$$\bar{T}\tilde{S} + \tilde{H} + \bar{u}\tilde{u} + \bar{v}\tilde{v} = \bar{u}r\hat{w}_x + \bar{v}r\hat{w}_r + \bar{v}\hat{w} \tag{2.26}$$

$$\tilde{u}\bar{S}_x + \bar{u}\tilde{S}_x + \tilde{v}\bar{S}_r + \bar{v}\tilde{S}_r + \frac{2\hat{w}}{r}\tilde{S} = 0 \tag{2.27}$$

Equation (2.25) results from the combination of the derivatives of equations (2.13) and (2.14). The operator $\partial/\partial n$ is defined beneath equation (2.20). Equa-

tions (2.16), (2.17), (2.20), (2.21), and (2.23) to (2.27) form a system of nine equations and nine unknowns: $\bar{u}$, $\bar{v}$, $\hat{w}$, $\bar{H}$, $\bar{S}$, $\tilde{u}$, $\tilde{v}$, $\tilde{H}$, and $\tilde{S}$. The first set, equations (2.16), (2.17), (2.20), and (2.21), are coupled weakly to the second set, equations (2.23) to (2.27), through the term $(1/r)(\partial w/\partial\phi)$ in equation (2.17).

The method of characteristics (ref. 24) is applied to equations (2.17) and (2.20) and results in the following characteristic equations:

$$\cot\mu\,\frac{dq}{q} \mp d\bar{\theta} + \frac{\cot\mu}{q^2}\left(\bar{T}\,d\bar{S} - d\bar{H}\right) - \frac{\sin\mu\,dr}{\sin(\bar{\theta}\pm\mu)}\left[\sin\bar{\theta}\left(\frac{1}{r}+\frac{\bar{g}}{a^2}\right)+\frac{\hat{w}}{\bar{q}r}\right] = 0 \tag{2.28}$$

These equations are valid along the characteristic directions

$$\frac{dr}{dx} = \tan(\bar{\theta}\pm\mu) \tag{2.29}$$

where $\bar{q} = \sqrt{\bar{u}^2+\bar{v}^2}$, $\bar{\theta}$ (the direction of the flow) $= \tan^{-1}(\bar{v}/\bar{u})$, and μ (the Mach angle) $= \sin^{-1}(1/M)$.

A second set of compatibility equations are derived from equations (2.24) and (2.25). Equation (2.24) is expressed as

$$\left(1-\frac{\bar{u}^2}{\bar{a}^2}\right)\tilde{u}_x + \left(1-\frac{\bar{v}^2}{\bar{a}^2}\right)\tilde{v}_r - \frac{\bar{u}\bar{v}}{\bar{a}^2}\left(\tilde{u}_r+\tilde{v}_x\right) = \mathcal{F} \tag{2.30}$$

where $\mathcal{F}$ stands for the right-hand side of equation (2.24) rewritten in the form

$$\mathcal{F} = -\frac{\tilde{v}}{r}+\frac{\hat{w}}{r}+\frac{1}{\bar{a}^2}\left[\bar{q}\tilde{u}\left(-\frac{\partial q}{\partial x}+\frac{\partial\bar{u}}{\partial\sigma}\right)+\tilde{qv}\left(\frac{\partial\bar{q}}{\partial r}+\frac{\partial\bar{v}}{\partial\sigma}\right)\right.$$
$$+\frac{2\hat{w}}{r}\left(\bar{T}\tilde{S}-\tilde{H}+2\bar{u}\tilde{u}+2\bar{v}\tilde{v}-\bar{v}\hat{w}+\hat{w}^2\right)$$
$$\left.+g\left(\bar{v}-\tilde{v}+2\hat{w}+\bar{v}\,\frac{\tilde{a}^2}{\bar{a}^2}\right)-\tilde{a}^2M^2\,\frac{\partial q}{\partial\sigma}\right]$$

in which $\partial/\partial\sigma$ is the derivative along the streamline defined by $q\partial/\partial\sigma = u(\partial/\partial x) + v(\partial/\partial r)$. Then equations (2.25) and (2.30) yield a second set of compatibility equations

$$d\tilde{u} + \tan(\bar{\theta} \mp \mu)\, d\tilde{v} = \frac{\sin\mu\, dr}{\sin(\bar{\theta} \pm \mu)\cos(\theta \mp \mu)}(\pm J\cos\mu - \mathcal{G}\sin\mu) \tag{2.31}$$

along the same characteristic directions

$$\frac{dr}{dx} = \tan(\bar{\theta} \bullet \mu) \tag{2.32}$$

where J represents the right-hand side of equation (2.25).

Equations (2.28), (2.16), and (2.21) provide solutions for $\bar{u}$, $\bar{v}$, $\bar{S}$, and $\bar{H}$ for a given value of $\hat{w}$, and equations (2.31), (2.23), (2.26), and (2.27) yield $\tilde{u}$, $\tilde{v}$, $\tilde{S}$, $\tilde{H}$, and $\hat{w}$. Solutions are obtained by simultaneously solving for the velocity components at the characteristic intersections and for enthalpy and entropy along streamlines.

2.2 Shock Conditions

The treatment of the bow shock and all embedded shocks is approached in the same manner. When the complete set of five shock equations are limited to the plane $\phi = 0$, the ϕ-momentum equation vanishes indentically. There are four remaining equations to solve for the shock shape $\bar{f}_r$ and $\bar{u}$, $\bar{v}$, $\bar{p}$, and $\bar{T}$ behind the shock.

The compatibility condition along the C^+ characteristic behind the shock provides the additional equation needed to close the system for the axisymmetric case. The equations needed to determine $\tilde{u}$, $\tilde{v}$, $\hat{w}$, $\tilde{T}$, and $\tilde{p}$ are derived by taking the first derivative with respect to ϕ of the ϕ-momentum equation across the shock and the second derivative with respect to ϕ of the remaining shock equations. (The procedure for deriving these shock equations is described in detail in Section 3.) This process introduces six unknowns, $\tilde{u}$, $\tilde{v}$, $\hat{w}$, $\tilde{p}$, $\tilde{T}$, and $\tilde{f}$, and five new equations. The compatibility equation for the second derivative quantities, equation (2.31), is used to close the system behind the shock.

2.3 Method of Solution

Because the two sets of equations are coupled only weakly through $\hat{w}$, the method of solution is iterative. A value of $\hat{w}$ is assumed, and the system consisting of equations (2.16), (2.21), and (2.28) is solved for $\bar{u}$, $\bar{v}$, $\bar{H}$, and $\bar{S}$. This information is used to solve the second set of equations for $\tilde{u}$, $\tilde{v}$, $\tilde{H}$, $\tilde{S}$, and $\hat{w}$. The entire procedure is repeated until the value of $\hat{w}$ converges.

The program is an extrapolation program, and it requires initial input approximately one body length from the axis of the aircraft. These data must be provided either by experimental methods or by programs which calculate the entire flow field about an aircraft. From the first data points on the initial line, a new bow shock point is located. Calculations proceed from this point along the C^- characteristic until the initial data line is intersected. Thus, a new data line is created. This

process is repeated until finally the new data line is a C^- characteristic which terminates at the last data point on the initial line. The next C^- characteristic is then started, and calculations continue to ground intersection. (See sketch B.)

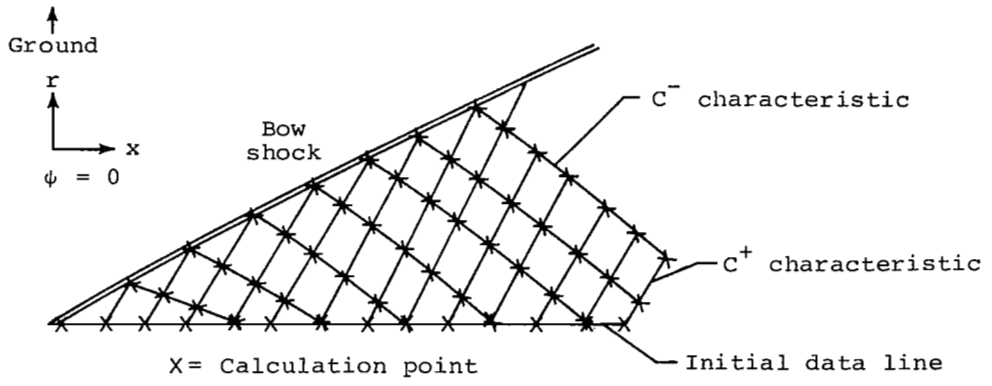

Sketch B

2.4 Far-Field Modifications

Because of the extreme propagation distances necessary with this method and thus the possibility of accumulated error in many steps taken, the outgoing $\theta + \mu$ characteristics are modified according to Whitham theory to allow for a gradual increase of step size in C^+ to the order of several body lengths as r increases. Within this modification, the characteristics are no longer considered to be straight but are curved in a manner consistent with Whitham theory. The modification is applied at each step in the $\theta + \mu$ characteristic and along the shock waves.

Whitham (ref. 4) gives the following relationship for the slope of the characteristic

$$\frac{dx}{dr} = \beta_\infty - \frac{k_\infty F}{2r^{1/2}}$$

where

$$\beta_\infty = \sqrt{M_\infty^2 - 1} \qquad k_\infty = \frac{\gamma + 1}{\gamma} \frac{M_\infty^2}{\beta_\infty} \qquad F = r^{1/2} \frac{\nabla p}{p}$$

The exact characteristic is modified by

$$\frac{dx}{dr} - \beta_\infty + \frac{k_\infty F}{2r^{1/2}} = \cot(\theta + \mu) - \beta_\infty + \frac{k_\infty F}{2r^{1/2}}$$

The characteristic equation is then rearranged so that the left side is an exact differential of the invariant under Whitham theory, and the right side is then an order of magnitude smaller than that in a standard characteristic equation

$$d\left(x - \beta_\infty r + k_\infty F r^{1/2}\right) = \left[\cot(\theta + \mu) - \beta_\infty + \frac{k_\infty F}{2r^{1/2}}\right] dr \tag{2.33}$$

Thus,

$$x = \beta_\infty r - k_\infty F r^{1/2} + \int E\, dr + A_c$$

where

$$E = \cot(\theta + \mu) - \beta_\infty + \frac{k_\infty F}{2r^{1/2}}$$

and A_c is a constant of integration. E is smaller than $\cot(\theta + \mu)$ and thus allows the step size to gradually increase to several body lengths in the far field. A similar procedure is used for the bow shock and for embedded shocks. A more detailed description of this procedure is found in reference 1. It is determined in reference 1 that errors of less than 1 percent are present in ground signatures even when the radial step sizes are allowed to increase gradually to several body lengths in the far field.

3. COALESCENCE OF SHOCKS

3.1 Axisymmetric Shock Coalescence

3.1.1 Governing equations.- Once removed from the axis of the body, the treatment of the shock interaction for the axisymmetric case becomes the same as for the two-dimensional case. Thus, when the shock angle is defined, the oblique shock equations may be used.

Incoming shocks $f_1(r)$ and $f_2(r)$ are given, and it is assumed that the point of intersection p_o has already been determined. (See sketch C.) Theory tells us

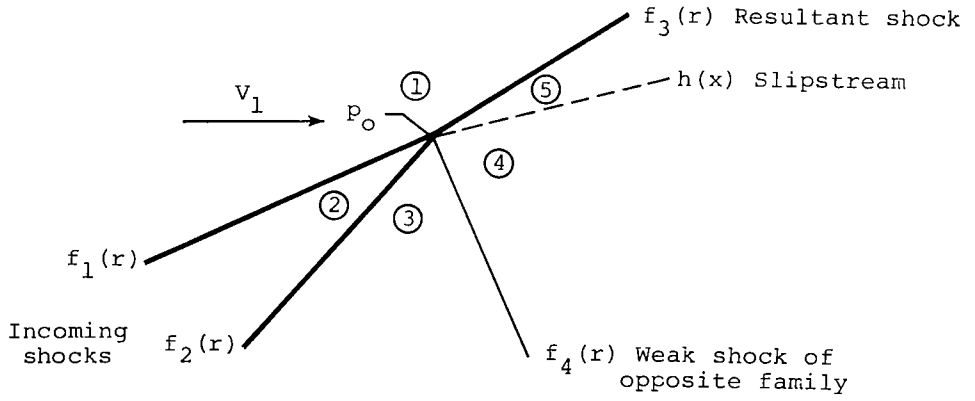

Sketch C

that from a shock-shock interaction of this nature, we may expect a resultant shock $f_3(r)$ of the same family, and a slipstream h created because of the difference in entropy of the flow passing through one shock and that passing through two shocks. Because the pressure and flow direction must be equal at the slipstream, a weak (isentropic) expansion or shock $f_4(r)$ of the opposite family may be needed to allow both conditions to be met.

In this situation, the unknowns are u_4, v_4, p_4, T_4, v_5, u_5, p_5, T_5, β_3, and β_4, where β is the shock angle with respect to the flow ahead. The standard oblique shock equations are

$$\frac{u_{1,n}}{u_{5,n}} = \frac{6M_{1,n}}{M_{1,n}^2 + 5} \tag{3.1}$$

$$\frac{p_5}{p_1} = \frac{7M_{1,n}^2 - 1}{6} \tag{3.2}$$

$$v_{1,t} = v_{5,t} \tag{3.3}$$

$$\frac{T_5}{T_1} = \frac{\left(7M_{1,n}^2 - 1\right)\left(M_{1,n}^2 + 5\right)}{36M_{1,n}^2} \tag{3.4}$$

The conditions holding across the slipstream $h(x)$ are

$$\theta_4 = \theta_5 \tag{3.5}$$

and

$$p_4 = p_5 \tag{3.6}$$

and across the isentropic wave in regions 3 and 4, we require

$$T_{4,T} = T_{3,T} \tag{3.7}$$

$$p_{4,T} = p_{3,T} \tag{3.8}$$

$$\frac{p}{p_T} = \left(1 + \frac{M^2}{5}\right)^{-7/2} \tag{3.9}$$

$$\frac{T}{T_T} = \left(1 + \frac{M^2}{5}\right)^{-1} \tag{3.10}$$

The system consisting of equations (3.1) to (3.10) is closed with 10 equations and 10 unknowns. All values in regions 1 and 3 are known.

3.1.2 Method of solution.- The solution process is begun by assuming an initial value of β_3; the guess used is

$$\beta_3 = (\beta_1 + \beta_2)/2$$

Using equations (3.1) to (3.4), u_5, p_5, v_5, and T_5 are calculated. From equations (3.5) and (3.6), values for θ_4 and p_4 are obtained. Because total pressure and total temperature in regions 3 and 4 are equal and because all information in region 3 is known, equation (3.9) may be applied in both regions to calculate

$$M_4^2 = 5\left[\left(1.0 + 0.2M_3^2\right)\left(\frac{p_3}{p_4}\right)^{2/7} - 1.0\right] \tag{3.11}$$

and equation (3.10) can be used to calculate

$$T_4 = \frac{T_3\left[1.0 + \left(M_3^2/5\right)\right]}{1.0 + \left(M_4^2/5\right)} \tag{3.12}$$

Since this is a perfect gas

$$a_4 = \sqrt{\gamma RT} \tag{3.13}$$

$$u_4 = \frac{a_4 M_4}{\sqrt{1 + \tan^2\theta_4}} \tag{3.14}$$

and

$$v_4 = u_4 \tan\theta_4 \tag{3.15}$$

The Prandtl-Meyer angle in both regions is

$$\nu_4 = \left(\frac{\gamma + 1}{\gamma - 1}\right)^{1/2} \tan^{-1}\left[\left(\frac{\gamma - 1}{\gamma + 1}\right)\left(M_4^2 - 1\right)\right]^{1/2} - \tan^{-1}\left(M_4^2 - 1\right)^{1/2} \tag{3.16}$$

$$\nu_3 = \left(\frac{\gamma + 1}{\gamma - 1}\right)^{1/2} \tan^{-1}\left[\left(\frac{\gamma - 1}{\gamma + 1}\right)\left(M_3^2 - 1\right)\right]^{1/2} - \tan^{-1}\left(M_3^2 - 1\right)^{1/2} \tag{3.17}$$

The angle of the weak wave f_4 is calculated using the standard pressure ratio equation

$$\beta_4 = \sin^{-1}\left[\left(\frac{\frac{6p_4}{p_3} + 1.0}{7M_3^2}\right)^{1/2}\right] \tag{3.18}$$

It has already been determined that the wave f_4 must be of the opposite family. If it is an expansion, then $p_4 < p_3$, and therefore, $M_4 > M_3$ and $\nu_4 > \nu_3$. Also, because it is of the opposite family, then $\theta_4 > \theta_3$. Similarly, if it is a shock, then $p_4 > p_3$, $M_4 < M_3$, $\nu_4 < \nu_3$, and $\theta_4 < \theta_3$. The error in the original guess β_3 is assessed by calculating

$$\text{Error(N)} = (\nu_4 - \nu_3) + (\theta_3 - \theta_4) \tag{3.19}$$

To iterate, a new value of β is assumed, and all calculations are repeated. After the second iteration, a straight line extrapolation is used to guess a new value of $\beta_3(N)$

$$\beta_3(N) = \frac{\text{Error(N-2)}\ \beta_3(N-1) - \text{Error(N-1)}\ \beta_3(N-2)}{\text{Error(N-2)} - \text{Error(N-1)}} \tag{3.20}$$

where N represents successive iterations after the second. Iterations are continued until

$$\text{Error(N)} < \varepsilon$$

where ε is some predetermined error criterion. Generally, convergence occurs within five or six iterations even when the error criterion ε is on the order of 10^{-10} for weak shocks. Once the angles β_3 and β_4 have been determined, the entropies S_4 and S_5 may be calculated using standard shock equations. The slopes of the shocks and slipstream are

$$f_{3_r} = \frac{1}{\tan(\beta_3 + \theta_1)} \tag{3.21}$$

$$f_{4_r} = \frac{1}{\tan(\beta_4 + \theta_3)} \tag{3.22}$$

and

$$h_x = \tan^{-1}\left(\frac{v_4}{u_4}\right) \tag{3.23}$$

3.2 Asymmetric Shock Coalescence

3.2.1 Derivation of shock equations.- The shock conditions across the resultant embedded shock $x = f_3(r,\psi)$ are now developed. The region ahead of the shock is denoted by the subscript 1 and that immediately behind the shock by the subscript 5. The conservation conditions across the shock are

Mass

$$\rho_1\left(u_1 - v_1 f_{3_r} - \frac{w_1 f_{3_\psi}}{r}\right) = \dot{m} = \rho_5\left(u_5 - v_5 f_{3_r} - \frac{w_5 f_{3_\psi}}{r}\right) \tag{3.24}$$

Momentum

$$mu_1 + p_1 = mu_5 + p_5 \tag{3.25}$$

$$u_1 f_{3_r} + v_1 = u_5 f_{3_r} + v_5 \tag{3.26}$$

$$u_1 \frac{f_{3_\psi}}{r} + w_1 = u_5 \frac{f_{3_\psi}}{r} + w_5 \tag{3.27}$$

Energy

$$u_1^2 + v_1^2 + w_1^2 + \frac{2\gamma RT_1}{\gamma - 1} = u_5^2 + v_5^2 + w_5^2 + \frac{2\gamma RT_5}{\gamma - 1} \tag{3.28}$$

To avoid difficulty as the shock strength becomes weak, these equations were rearranged in reference 3 to yield the following three governing equations:

$$(u_5 - u_1) f_{3_r} + v_5 - v_1 = 0 \tag{3.29}$$

$$(u_5 - u_1) \frac{f_{3_\psi}}{r} + w_5 - w_1 = 0 \tag{3.30}$$

and

$$(\gamma + 1)\varrho_1\varrho_5 - (\gamma - 1)\varrho_1^2 = 2\gamma RT_1\left(1 + f_{3_r}^2 + \frac{f_{3_\psi}^2}{r^2}\right) \tag{3.31}$$

where

$$Q_i = u_i - v_i f_{3_r} - \frac{w_i f_{3_\phi}}{r}$$

These three equations are used to provide solutions for u, v, and f_r in the plane of symmetry. To determine p and T, equations (3.25) and (3.28) must be used.

The asymmetric shock conditions are developed when each of these equations is differentiated twice along the shock surface with respect to ϕ, and then ϕ is set equal to 0 to reflect conditions in the plane of symmetry. In the plane $\phi = 0$, the first derivatives with respect to ϕ of all variables and shock surfaces vanish with the exception of w_ϕ. A detailed description of this derivation will be given for shock equation (3.29).

Let

$$A = (u_5 - u_1) f_{3_r} + v_5 - v_1 = 0$$

The derivative along the shock surface $x = f_3(r,\phi)$ with respect to ϕ is

$$\frac{\partial}{\partial \phi} = \frac{\partial f_3}{\partial \phi} \frac{\partial}{\partial x} + \frac{\partial}{\partial \phi}$$

The first derivative with respect to ϕ is

$$\frac{\partial A}{\partial \phi} = \frac{\partial A}{\partial x} f_{3_\phi} + \frac{\partial A}{\partial \phi} = A_x f_{3_\phi} + A_\phi$$

The second derivative then yields

$$\frac{\partial^2 A}{\partial \phi^2} = \frac{\partial}{\partial x}\left(A_x f_{3_\phi} + A_\phi\right) f_{3_\phi} + \frac{\partial}{\partial \phi}\left(A_x f_{3_\phi} + A_\phi\right)$$

Note immediately that the first term in this expression will vanish in the plane $\phi = 0$, since the factor f_{3_ϕ} vanishes. Thus, this term will not be expanded further. Working only with the second term, then

$$\frac{\partial}{\partial \phi}\left(A_x f_{3_\phi} + A_\phi\right) = A_{x\phi} f_{3_\phi} + A_x f_{3_{\phi\phi}} + A_{\phi\phi}$$

Again, the first term of this expression also vanishes in the plane $\phi = 0$. Therefore, in the plane $\phi = 0$

$$\frac{\partial^2 A}{\partial \phi^2} = A_x f_{3_{\phi\phi}} + A_{\phi\phi}$$

Expanding A_x and $A_{\phi\phi}$ yields

$$A_x = u_{5_x} f_{3_r} + u_5 f_{3_{rx}} - u_{1_x} f_{3_r} - u_1 f_{3_{rx}} + v_{5_x} - v_{1_x}$$

$$A_\phi = u_{5_\phi} f_{3_r} + u_5 f_{3_{r\phi}} - u_{1_\phi} f_{3_r} - u_1 f_{3_{r\phi}} + v_{5_\phi} - v_{1_\phi}$$

$$A_{\phi\phi} = u_{5_{\phi\phi}} f_{3_r} + u_{5_\phi} f_{3_{r\phi}} + u_{5_\phi} f_{3_{r\phi}} + u_5 f_{3_{r\phi\phi}} - u_{1_{\phi\phi}} f_{3_r}$$

$$+ u_{1_\phi} f_{3_{r\phi}} - u_{1_\phi} f_{3_{r\phi}} - u_1 f_{3_{r\phi\phi}} + v_{5_{\phi\phi}} - v_{1_{\phi\phi}}$$

In the plane $\phi = 0$

$$A_x = u_{5_x} f_{3_r} - u_{1_x} f_{3_r} + v_{5_x} - v_{1_x}$$

and

$$A_{\phi\phi} = u_{5_{\phi\phi}} f_{3_r} + u_5 f_{3_{r\phi\phi}} - u_{1_{\phi\phi}} f_{3_r} - u_1 f_{3_{r\phi\phi}} + v_{5_{\phi\phi}} - v_{1_{\phi\phi}}$$

Therefore

$$\left.\frac{\partial^2 A}{\partial \phi^2}\right|_{\phi=0} = \left(u_{5_x} f_{3_r} - u_{1_x} f_{3_r} + v_{5_x} - v_{1_x}\right) f_{3_{\phi\phi}} + u_{5_{\phi\phi}} f_{3_r}$$

$$+ u_5 f_{3_{r\phi\phi}} - u_{1_{\phi\phi}} f_{3_r} - u_1 f_{3_{r\phi\phi}}$$

The bar ($\bar{}$) and tilde ($\tilde{}$) over symbols denote values in the vertical plane $\phi = 0$. Thus, the asymmetric version of equation (3.29) becomes

$$\left(\bar{u}_{5_x}\bar{f}_{3_r} - \bar{u}_{1_x}\bar{f}_{3_r} + \bar{v}_{5_x} - \bar{v}_{1_x}\right)\tilde{f}_3 + \left(\tilde{u}_5\bar{f}_{3_r} + \bar{u}_5\tilde{f}_{3_r} - \tilde{u}_1\bar{f}_{3_r} - \bar{u}_1\tilde{f}_{3_r} + \tilde{v}_5 - \tilde{v}_1\right) = 0 \tag{3.32}$$

By a similar method, equation (3.30) becomes

$$\hat{w}_5 = \frac{\tilde{f}_3(\bar{u}_1 - \bar{u}_5)}{r} + \hat{w}_1 \tag{3.33}$$

where

$$\hat{w} = \frac{\left.\frac{\partial w}{\partial \psi}\right|_{\psi=0}}{U_\infty}$$

and equation (3.31) becomes

$$2\gamma R\left[\left(\bar{T}_{1_x}\tilde{f}_3 + \tilde{T}_1\right)\left(1 + \bar{f}_{3_r}^2\right)\right] + 4\gamma R T_1\left(\bar{f}_{3_r}\tilde{f}_{3_r} + \frac{\tilde{f}_3^2}{r^2}\right)$$

$$= (\gamma + 1)\left(\tilde{Q}_1\bar{Q}_5 + \bar{Q}_1\tilde{Q}_5\right) - 2(\gamma - 1)\bar{Q}_1\tilde{Q}_1 \qquad (3.34)$$

where

$$\tilde{Q}_i = \bar{u}_{i_x}\tilde{f}_3 - \bar{v}_{i_x}\bar{f}_{3_r}\tilde{f}_3 + \tilde{u}_i - \tilde{v}_i\bar{f}_{3_r} - \bar{v}_i\tilde{f}_{3_r} - \frac{2\hat{w}_i}{r}$$

and

$$\bar{Q}_i = \bar{u}_i - \bar{v}_i\bar{f}_{3_r} \qquad (i = 1,5)$$

3.2.2 Asymmetric analysis.- The three-dimensional geometry of the shock coalescence is described by sketch D, and the geometry in the plane $\psi = 0$, by sketch E.

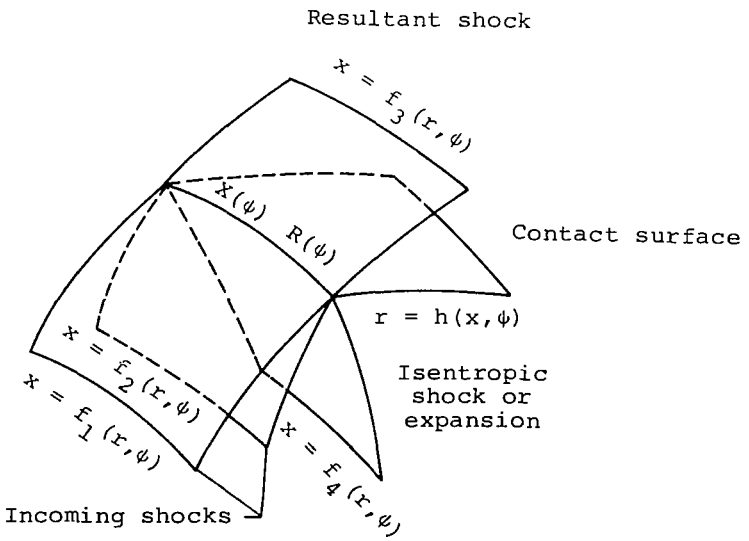

Sketch D

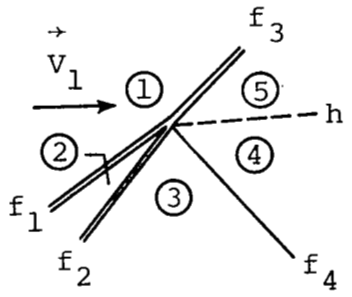

Sketch E

Incoming shock waves $x = f_1(r,\phi)$ and $x = f_2(r,\phi)$ coalesce to form the following system: resultant shock wave $x = f_3(r,\phi)$, slipstream $r = h(x,\phi)$, and a weak (isentropic) wave of the opposite family $x = f_4(r,\phi)$. This results in five surfaces intersecting along the line $x = X(\phi)$, $r = R(\phi)$. Taking the second derivative along each of the intersecting surfaces with respect to ϕ and setting ϕ equal to 0 yields

$$\tilde{X} = \bar{f}_{j_r}\tilde{R} + \tilde{f}_j \qquad (j = 1,2,3,4) \tag{3.35}$$

$$\tilde{R} = \bar{h}_x\tilde{X} + \tilde{h} \tag{3.36}$$

Along the slipstream surface $r = h(x,\phi)$, pressures and flow direction on either side are the same. Thus,

$$p_4 = p_5$$

$$\vec{V}_4 \cdot \hat{n} = 0$$

$$\vec{V}_5 \cdot \hat{n} = 0$$

where $\hat{n}$ is the normal to the slipstream defined by

$$\hat{n} = \hat{j} - h_x\hat{i} - h_\phi \frac{\hat{\phi}}{r}$$

The equations for flow direction at the surface h become

$$-u_i h_x + v_i - w_i \frac{h_\phi}{r} = 0 \qquad (i = 4, 5)$$

Second derivatives along the slipstream surface with respect to ψ are calculated by using

$$\frac{\partial^2}{\partial\psi^2} = h_{\psi\psi}\frac{\partial}{\partial r} + \frac{\partial^2}{\partial\psi^2}$$

and thus the pressure equation yields

$$\bar{p}_{4_r}\tilde{h} + \tilde{p}_4 = \bar{p}_{5_r}\tilde{h} + \tilde{p}_5 \tag{3.37}$$

and the flow equations

$$-\bar{u}_{4_r}\bar{h}_x\tilde{h} + \bar{v}_{4_r}\tilde{h} - \tilde{u}_4\bar{h}_x - \bar{u}_4\tilde{h}_x + \tilde{v}_4 - \frac{2\hat{w}_4\tilde{h}}{r} = 0 \tag{3.38a}$$

$$-\bar{u}_{5_r}\bar{h}_x\tilde{h} + \bar{v}_{5_r}\tilde{h} - \tilde{u}_5\bar{h}_x - \bar{u}_5\tilde{h}_x + \tilde{v}_5 - \frac{2\hat{w}_5\tilde{h}}{r} = 0 \tag{3.38b}$$

The three shock equations for the asymmetric quantities (eqs. (3.32) to (3.34)) were derived in the previous section and are valid from regions 1 to 5 across shock f_3. To calculate T behind the shock, the original energy shock equation (eq. (3.28)) may be used. Taking the second derivative of this equation with respect to ψ and setting ψ equal to 0 yields

$$\left[2\bar{u}_5\bar{u}_{5_x} - 2\bar{u}_1\bar{u}_{1_x} + 2\bar{v}_5\bar{v}_{5_x} - 2\bar{v}_1\bar{v}_{1_x} + \frac{2\gamma}{\gamma-1}\left(\bar{T}_{5_x} - \bar{T}_{1_x}\right)\right]\tilde{f}_3$$

$$+ \left[2\bar{u}_5\tilde{u}_5 - 2\bar{u}_1\tilde{u}_1 + 2\hat{w}_5^2 - 2\hat{w}_1^2 + 2\bar{v}_5\tilde{v}_5 - 2\bar{v}_1\tilde{v}_1\right.$$

$$\left. + \left(\frac{2\gamma}{\gamma-1}\right)\left(\tilde{T}_5 - \tilde{T}_1\right)\right] = 0 \tag{3.39}$$

To compute $\tilde{s}_5$ across the shock f_3, the method in reference 2 is used

$$\tilde{s}_5 = \tilde{s}_1 - \left(\bar{s}_{5_x} - \bar{s}_{1_x}\right)\tilde{f}_3 + \frac{d}{dM_{1,n}^2}\frac{\Delta s_{sh}}{R} - \widetilde{M_1^2 \sin^2\beta} \tag{3.40}$$

where ΔS_{sh} is the jump in entropy across the shock,

$$\widetilde{M_1^2 \sin^2\beta} = \frac{\left(q_1^2/H_\infty^2\right)\sin^2\beta}{a^{-2}} + \left(q_1^2 \sin^2\beta\right)\frac{\tilde{a}_1^2}{\bar{a}_1^{-4}}$$

$$= \frac{2\left(\bar{u}_1 - \bar{v}_1\tilde{f}_{3_r}\right)\left[\tilde{u}_1 - \tilde{v}_1\bar{f}_{3_r} + \left(\bar{u}_{1_x} - \bar{v}_{1_x}\bar{f}_{3_r}\right)\tilde{f}_3 - \bar{v}_1\tilde{f}_{3_r} - \left(2\hat{w}\tilde{f}_3/r\right)\right]}{\left(1 + \bar{f}_{3_r}^2\right)\bar{a}_1^2}$$

$$- \frac{\left(\bar{u}_1 - \bar{v}_1\bar{f}_{3_r}\right)^2\left[2\bar{f}_{3_r}\tilde{f}_{3_r} + \left(2\tilde{f}_3^2/r^2\right)\right]}{\left(1 + \bar{f}_{3_r}^2\right)^2\bar{a}_1^2}$$

$$- \frac{\left(\bar{u}_1 - \bar{v}_1\bar{f}_{3_r}\right)^2}{1 + \bar{f}_{3_r}^2}\frac{\tilde{a}_1^2}{\bar{a}_1^4}$$

and

$$\overline{\frac{d}{dM_{1,n}^2}\frac{\Delta S_{sh}}{R}} = \left(\frac{2\gamma}{\gamma - 1}\right)\frac{1}{2\gamma M_1^2 \sin^2\beta - (\gamma - 1)} - \frac{\gamma}{\gamma - 1}\left[\frac{1}{M_1^2 \sin^2\beta}\right.$$

$$\left. - \frac{\gamma - 1}{M_1^2 \sin^2\beta\,(\gamma - 1) + 1}\right]$$

$$= \frac{\gamma}{\gamma - 1}\left\{\frac{1}{\gamma M_1^2 \sin^2\beta - \frac{\gamma - 1}{2}} - \frac{1}{\left(M_1^2 \sin^2\beta\right)\left[M_1^2 \sin^2\beta\left(\frac{\gamma - 1}{2}\right) + 1\right]}\right\}$$

From the relation

$$dS = c_p\frac{dT}{T} - R\frac{dp}{p}$$

one gets

$$\tilde{s} = \left[\left(\frac{\gamma}{\gamma - 1}\right)\frac{\bar{T}_x}{\bar{T}} - \frac{\bar{p}_x}{\bar{p}}\right]\tilde{f} + \left(\frac{\gamma}{\gamma - 1}\right)\frac{\tilde{T}}{\bar{T}} - \frac{\tilde{p}}{\bar{p}}$$

This equation can then be used to get $\tilde{p}$ in region 5, or

$$\tilde{p}_5 = \frac{1}{\bar{p}_5}\left\{\left[\left(\frac{\gamma}{\gamma - 1}\right)\frac{\bar{T}_{5_x}}{\bar{T}_5} - \frac{\bar{p}_{5_x}}{\bar{p}_5}\right]\tilde{f}_3 + \left(\frac{\gamma}{\gamma - 1}\right)\frac{\tilde{T}_5}{\bar{T}_5} - \tilde{s}_5\right\} \tag{3.41}$$

For the examples shown in this paper, the surface $x = f_4(r,\phi)$ is an extremely weak (isentropic) shock or expansion wave across which the variables are nearly continuous. We therefore introduce the approximations that

$$u_3 = u_4$$

$$v_3 = v_4$$

$$p_3 = p_4$$

$$S_3 = S_4$$

$$T_3 = T_4$$

$$\hat{w}_3 = \hat{w}_4$$

Taking the second derivatives of the above relations along the weak surface f_4 yields the following five equations:

$$\bar{u}_{3_x}\tilde{f}_4 + \tilde{u}_3 = \bar{u}_{4_x}\tilde{f}_4 + \tilde{u}_4 \tag{3.42}$$

$$\bar{v}_{3_x}\tilde{f}_4 + \tilde{v}_3 = \bar{v}_{4_x}\tilde{f}_4 + \tilde{v}_4 \tag{3.43}$$

$$\bar{p}_{3_x}\tilde{f}_4 + \tilde{p}_3 = \bar{p}_{4_x}\tilde{f}_4 + \tilde{p}_4 \tag{3.44}$$

$$\bar{s}_{3_x}\tilde{f}_4 + \tilde{s}_3 = \bar{s}_{4_x}\tilde{f}_4 + \tilde{s}_4 \tag{3.45}$$

$$\bar{T}_{3_x}\tilde{f}_4 + \tilde{T}_3 = \bar{T}_{4_x}\tilde{f}_4 + \tilde{T}_4 \tag{3.46}$$

and the following equation is retained for w:

$$\hat{w}_3 = \hat{w}_4 \tag{3.47}$$

The unknowns in the asymmetric system are $\tilde{X}$, $\tilde{R}$, $\tilde{f}_3$, $\tilde{f}_4$, $\tilde{h}$, $\tilde{f}_{3_r}$, $\tilde{h}_x$, $\tilde{u}_4$, $\tilde{v}_4$, $\hat{w}_4$, $\tilde{T}_4$, $\tilde{S}_4$, $\tilde{p}_4$, $\tilde{u}_5$, $\tilde{v}_5$, $\hat{w}_5$, $\tilde{T}_5$, $\tilde{S}_5$, and $\tilde{p}_5$. The equations valid in the system are the five intersection equations (eqs. (3.35) and (3.36)), the two slipstream equations (eqs. (3.37) and (3.38a)), the six shock equations (eqs. (3.32) to (3.34) and (3.39) to (3.41)), and the six continuity equations from regions 3 to 4 (eqs. (3.42) to (3.47)). There are 19 unknowns and 19 equations for the system. The system is closed. The slipstream flow equation (eq. (3.38b)) has been discarded because of the continuity approximations made across f_4. It is found that the approximation of continuity described above yields a rapidly converging solution whenever $\left|(P_4/P_3) - 1\right| < 10^{-5}$.

When $\left|(P_4/P_3) - 1\right| > 10^{-5}$, it is necessary to treat f_4 as a finite shock or expansion. If f_4 is a shock, then the complete set of shock equations (eqs. (3.32) to (3.34) and (3.39) to (3.41)) instead of equations (3.42) to (3.47), are applied from regions 3 to 4, equation (3.38b) is used, and a new unknown $\tilde{f}_{4_r}$ is introduced. The system then contains 20 equations and 20 unknowns. If f_4 is a finite expansion wave, the appropriate isentropic expansion equations are used.

3.2.3 Asymmetric solution process.- For the incoming shocks f_1 and f_2, the values of $\tilde{f}_{1_r}$, $\tilde{f}_{2_r}$, $\tilde{f}_1$, $\tilde{f}_2$, $\bar{f}_{1_r}$, and $\bar{f}_{2_r}$ are already known from the MMOC program. Equation (3.35) can be applied to shock surfaces 1 and 2 to solve for

$$\tilde{R} = \frac{\tilde{f}_2 - \tilde{f}_1}{\bar{f}_{1_r} - \bar{f}_{2_r}} \tag{3.48}$$

and

$$\tilde{X} = \bar{f}_{1_r}\tilde{R} + \tilde{f}_1 \tag{3.49}$$

Knowing $\tilde{X}$ and $\tilde{R}$, equations (3.35) and (3.36) may be applied to shock surfaces 3 and 4 to solve for

$$\tilde{f}_j = \tilde{X} - \bar{f}_{j_r}\tilde{R} \qquad (j = 3,\ 4) \tag{3.50}$$

and

$$\tilde{h} = \tilde{R} - \bar{h}_x\tilde{X} \tag{3.51}$$

where f_{3_r}, f_{4_r}, and h_x are known from the axisymmetric solution. Since everything is known in region 1, all bar ($\bar{}$) quantities are assumed known, and $\tilde{f}_3$ is now known, then equation (3.33) may be immediately used to solve for $\hat{w}_5$; i.e.,

$$\hat{w}_5 = \frac{\tilde{f}_3\left(\bar{u}_1 - \bar{u}_5\right)}{r} + \hat{w}_1 \tag{3.52}$$

Similarly, since all quantities in region 3 are known, equations (3.42) to (3.46) may be solved for the tilde ($\tilde{}$) variables in region 4. (If equation (3.47) is tested and the shock equations are needed at f_4, a double iteration procedure is used to determine an additional unknown $\tilde{f}_{4_r}$.) These quantities are

$$\tilde{u}_4 = \bar{u}_{3_x}\tilde{f}_4 + \tilde{u}_3 - \bar{u}_{4_x}\tilde{f}_4 \tag{3.53}$$

$$\tilde{v}_4 = \bar{v}_{3_x}\tilde{f}_4 + \tilde{v}_3 - \bar{v}_{4_x}\tilde{f}_4 \tag{3.54}$$

$$\tilde{p}_4 = \bar{p}_{3_x}\tilde{f}_4 + \tilde{p}_3 - \bar{p}_{4_x}\tilde{f}_4 \tag{3.55}$$

$$\tilde{T}_4 = \bar{T}_{3_x}\tilde{f}_4 + \tilde{T}_3 - \bar{T}_{4_x}\tilde{f}_4 \tag{3.56}$$

$$\tilde{s}_4 = \bar{s}_{3_x}\tilde{f}_4 + \tilde{s}_3 - \bar{s}_{4_x}\tilde{f}_4 \tag{3.57}$$

To solve for the other tilde ($\tilde{}$) variables in region 5, an initial guess is made for the value of $\tilde{f}_{3_r}$

$$\tilde{f}_{3_r} = 1/2\left(\tilde{f}_{1_r} + \tilde{f}_{2_r}\right)$$

Equations (3.32) and (3.34) are then used to solve for $\tilde{u}_5$ and $\tilde{v}_5$

$$\tilde{v}_5 = \frac{\left(\tilde{u}_1 - L_2 + L_3\right)\bar{f}_{3_r} + L_1}{1 + \bar{f}_{3_r}^2} \tag{3.58}$$

$$\tilde{u}_5 = \tilde{u}_1 + \frac{L_1 - \tilde{v}_5}{\bar{f}_{3_r}} \tag{3.59}$$

where

$$L_3 = \bar{v}_5\tilde{f}_{3_r} + \left(\bar{u}_{5_x} - \bar{v}_{5_x}\bar{f}_{3_r} - \frac{2\hat{w}_5}{r}\right)\tilde{f}_3$$

$$L_2 = \frac{B_5}{\left[(\gamma + 1)\bar{Q}_1\right]}$$

$$L_1 = \tilde{v}_1 + \left(\bar{u}_1 - \bar{u}_5\right)\tilde{f}_{3_r} + \left[\left(\bar{u}_{1_x} - \bar{u}_{5_x}\right)\bar{f}_{3_r} + \bar{v}_{1_x} - \bar{v}_{5_x}\right]\tilde{f}_3$$

$$B_5 = B_4 - B_3 + B_1 + B_2$$

$$B_4 = 2(\gamma - 1)\bar{Q}_1\tilde{Q}_1$$

$$B_3 = (\gamma + 1)\tilde{Q}_1\bar{Q}_5$$

$$B_2 = 4\bar{a}_1^2\left(\bar{f}_{3_r}\tilde{f}_{3_r} + \frac{\tilde{f}_3^2}{r^2}\right)$$

$$B_1 = 2\gamma\left(1 + \bar{f}_{3_r}^2\right)\left(\bar{T}_{1_x}\tilde{f}_3 + \tilde{T}_1\right)$$

$$\bar{Q}_5 = \bar{u}_5 - \bar{v}_5\bar{f}_{3_r}$$

$$\bar{Q}_1 = \bar{u}_1 - \bar{v}_1\bar{f}_{3_r}$$

$$\tilde{Q}_1 = \bar{u}_{1_x}\tilde{f}_3 - \bar{v}_{1_x}\bar{f}_{3_r}\tilde{f}_3 + \tilde{u}_1 - \tilde{v}_1\bar{f}_{3_r} - \bar{v}_1\tilde{f}_{3_r} - \frac{2\hat{w}_1\tilde{f}_3}{r}$$

Using equation (3.39), $\tilde{T}_5$ may be obtained as

$$\tilde{T}_5 = \tilde{T}_1 - \left[\left(\frac{\gamma - 1}{\gamma}\right)\left(\vartheta_1\tilde{f}_3 + \vartheta_2\right)\right] \tag{3.60}$$

where

$$\vartheta_1 = \bar{u}_5\bar{u}_{5_x} - \bar{u}_1\bar{u}_{1_x} + \bar{v}_5\bar{v}_{5_x} - \bar{v}_1\bar{v}_{1_x} + \left(\frac{\gamma}{\gamma - 1}\right)\left(\bar{T}_{5_x} - \bar{T}_{1_x}\right)$$

$$\vartheta_2 = \bar{u}_5\tilde{u}_5 - \bar{u}_1\tilde{u}_1 + \hat{w}_5^2 - \hat{w}_1^2 + \bar{v}_5\tilde{v}_5 - \bar{v}_1\tilde{v}_1$$

Equation (3.40) is used to solve for $\tilde{S}_5$, and equation (3.41), for $\tilde{p}_5$. The error in the iteration is evaluated by using equation (3.37)

$$\text{Error(N)} = \left(\bar{p}_{4_r} - \bar{p}_{5_r}\right)\tilde{h} + \tilde{p}_4 - \tilde{p}_5$$

A new guess for $\tilde{f}_{3_r}$ is made, for example,

$$\tilde{f}_{3_r}(2) = 1.1\tilde{f}_{3_r}(1)$$

and all variables from $\tilde{v}_5$ forward are recalculated with the new $\tilde{f}_{3_r}$. From the values $\tilde{f}_{3_r}(1)$, error (1), $\tilde{f}_{3_r}(2)$, and error (2), a straight line approximation is used to determine the new $\tilde{f}_{3_r}$

$$\tilde{f}_{3_r}(N) = \frac{\tilde{f}_{3_r}(N-2)\ \text{Error}(N-1) - \tilde{f}_{3_r}(N-1)\ \text{Error}(N-2)}{\text{Error}(N-1) - \text{Error}(N-2)}$$

The process is repeated until

$$\text{Error(N)} < \varepsilon$$

where ε is a predetermined error criterion. For the examples shown, even if ε is 10^{-10}, convergence occurs within five iterations. After convergence, equation (3.38b) is used to calculate h_x.

$$\tilde{h}_x = \frac{1}{\bar{u}_5}\left(-\bar{u}_{5_r}\bar{h}_x\tilde{h} + \bar{v}_{5_r}\tilde{h} - \tilde{u}_5\bar{h}_x + \tilde{v}_5 - \frac{2\hat{w}_5\tilde{h}}{r}\right) \tag{3.61}$$

If the shock equations are used at f_4, then equation (3.38a) is used to check convergence

$$-\bar{u}_{4_r}\bar{h}_x\tilde{h} + \bar{v}_{4_r}\tilde{h} - \tilde{u}_4\bar{h}_x - \bar{u}_4\tilde{h}_x + \tilde{v}_4 - \frac{2\hat{w}_4\tilde{h}}{r} = 0$$

The solution process for the asymmetric equations is summarized in the flow chart shown on the next page. The solid lines on this chart represent the case in which the wave f_4 is so weak that continuity may be assumed for u, v, p, T, S, and w. The dashed lines are used to represent the double iteration procedure which must be used when the shock equations are used at f_4. In that case,

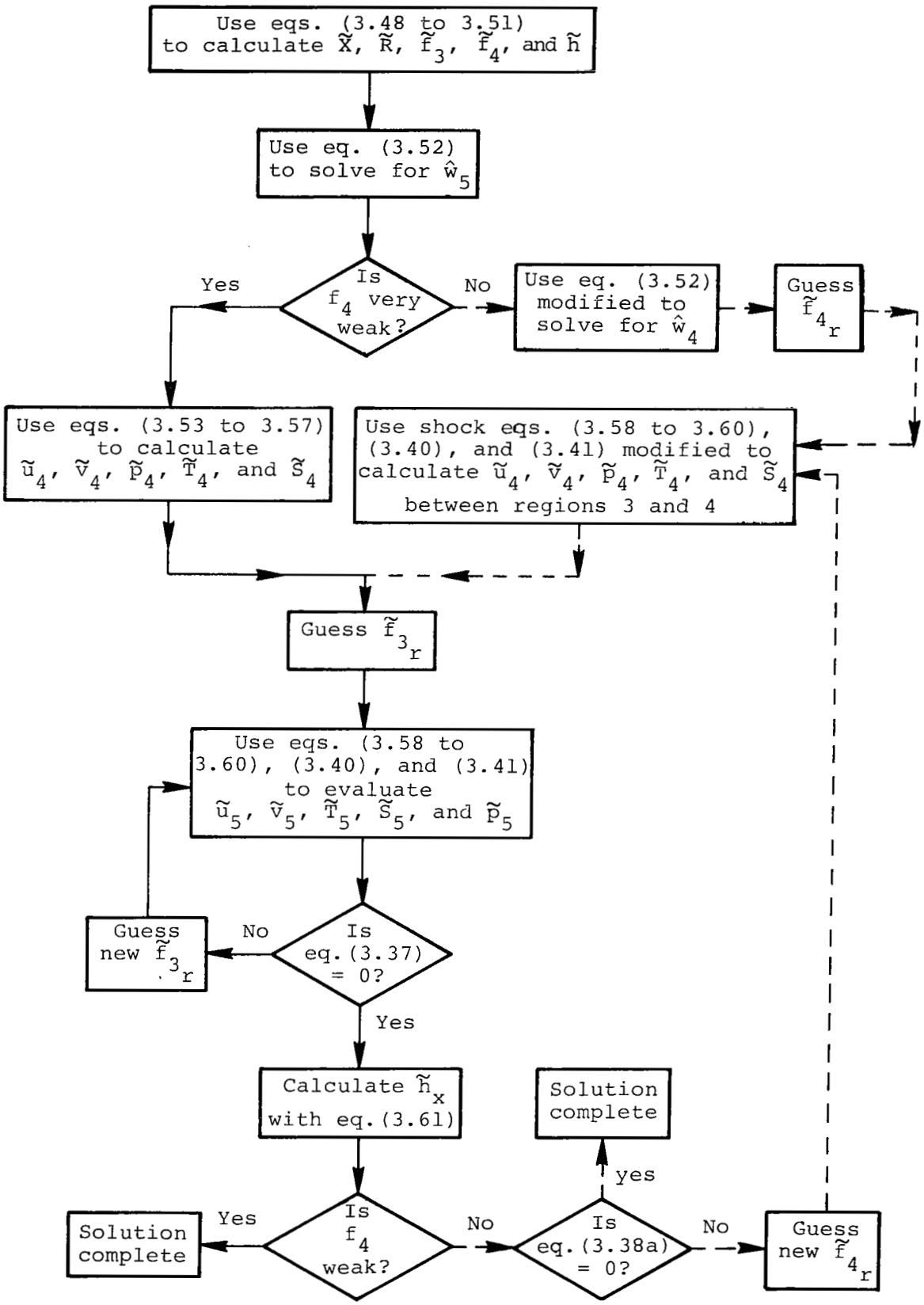
Use eqs. (3.48 to 3.51) to calculate $\tilde{X}$, $\tilde{R}$, $\tilde{f}_3$, $\tilde{f}_4$, and $\tilde{h}$
Use eq. (3.52) to solve for $\hat{w}_5$
Is f_4 very weak?
Yes
No
Use eq. (3.52) modified to solve for $\hat{w}_4$
Guess $\tilde{f}_{4_r}$
Use eqs. (3.53 to 3.57) to calculate $\tilde{u}_4$, $\tilde{v}_4$, $\tilde{p}_4$, $\tilde{T}_4$, and $\tilde{S}_4$
Use shock eqs. (3.58 to 3.60), (3.40), and (3.41) modified to calculate $\tilde{u}_4$, $\tilde{v}_4$, $\tilde{p}_4$, $\tilde{T}_4$, and $\tilde{S}_4$ between regions 3 and 4
Guess $\tilde{f}_{3_r}$
Use eqs. (3.58 to 3.60), (3.40), and (3.41) to evaluate $\tilde{u}_5$, $\tilde{v}_5$, $\tilde{T}_5$, $\tilde{S}_5$, and $\tilde{p}_5$
Guess new $\tilde{f}_{3_r}$
No
Is eq. (3.37) = 0?
Yes
Calculate $\tilde{h}_x$ with eq. (3.61)
Solution complete
yes
Is f_4 weak?
Yes
Solution complete
No
Is eq. (3.38a) = 0?
No
Guess new $\tilde{f}_{4_r}$

equations (3.53) to (3.57) must be replaced by equations comparable to equations (3.52), (3.58) to (3.60), (3.40), and (3.41)) to solve from regions 3 to 4.

4. SPATIAL DERIVATIVES NEEDED FOR ASYMMETRIC SOLUTION

4.1 Spatial Derivatives in Regions 4 and 5

The system of equations for nonaxisymmetric shock coalescence (eqs. (3.24) to (3.47)) is a closed system with the assumption that all spatial derivatives of u, v, p, and T are known. The method used to obtain these derivatives in regions 4 and 5 is now explained.

In region 5, the following four governing flow equations are valid:

x-Momentum

$$\bar{p}_5\bar{u}_5\bar{u}_{5_x} + \bar{p}_5\bar{v}_5\bar{u}_{5_r} + \bar{T}_5\bar{p}_{5_x} = 0 \tag{4.1}$$

r-Momentum

$$\bar{p}_5\bar{u}_5\bar{v}_{5_x} + \bar{p}_5\bar{v}_5\bar{v}_{5_r} = -\bar{g}\bar{p}_5 - R\bar{T}_5\bar{p}_{5_r} \tag{4.2}$$

Continuity

$$\bar{p}_5\bar{T}_5\bar{u}_{5_x} + \bar{p}_5\bar{T}_5\bar{v}_{5_r} - \bar{u}_5\bar{p}_5\bar{T}_{5_x} - \bar{v}_5\bar{p}_5\bar{T}_{5_r}$$

$$+ \bar{u}_5\bar{T}_5\bar{p}_{5_x} + \bar{v}_5\bar{T}_5\bar{p}_{5_r} = -\frac{\bar{p}_5\bar{T}_5}{r}\left(\hat{w}_5 + \bar{v}_5\right) \tag{4.3}$$

Energy

$$\bar{u}_5^2\bar{T}_5\bar{u}_{5_x} + \bar{u}_5\bar{v}_5\bar{v}_{5_x} + \bar{u}_5\bar{v}_5\bar{u}_{5_r} + \bar{v}_5^2\bar{v}_{5_r} + \frac{\gamma}{\gamma - 1}\bar{u}_5\bar{T}_{5_x} + \frac{\gamma}{\gamma - 1}\bar{v}_5\bar{T}_{5_r} = \bar{g}\bar{v}_5 \tag{4.4}$$

Because of the weakness of the wave between regions 3 and 4 and the continuity assumption made, $f_{4_{rr}}$ does not appear as an unknown in the system. We therefore apply only three flow equations in region 4 - the two momentum equations and the

continuity equation. The energy equation is used only as a check for the continuity assumption. The equations in region 4 are

$$\bar{p}_4\bar{u}_4\bar{u}_{4_x} + \bar{p}_4\bar{v}_4\bar{u}_{4_r} + \bar{T}_4\bar{p}_{4_x} = 0 \tag{4.5}$$

$$\bar{p}_4\bar{u}_4\bar{v}_{4_x} + \bar{p}_4\bar{v}_4\bar{v}_{4_r} + R\bar{T}_4\bar{p}_{4_r} = -\bar{g}\bar{p}_4 \tag{4.6}$$

$$\bar{p}_4\bar{T}_4\bar{u}_{4_x} + \bar{p}_4\bar{T}_4\bar{v}_{4_r} - \bar{u}_4\bar{p}_4\bar{T}_{4_x} - \bar{v}_4\bar{p}_4\bar{T}_{4_r} + \bar{u}_4\bar{T}_4\bar{p}_{4_x} + \bar{v}_4\bar{T}_4\bar{p}_{4_r} = -\frac{\bar{p}_4\bar{T}_4}{r}\left(\hat{w}_4 + \bar{v}_4\right) \tag{4.7}$$

The other equations needed for this system are derived by using the principle that the tangential derivatives of the shock conservation conditions across a wave are continuous and a theory developed by Lin and Rubinov in reference 21, which shows that if the curvature of a shock is known, then the spatial derivatives of the hydrodynamical properties behind the shock can be found.

Looking first at the weak wave f_4, it has already been established that the properties u, v, p, T, and S are continuous across this wave for the case considered. The tangential derivative along the wave $x = f_4(r)$ is

$$\frac{\partial}{\partial x}(\,)f_{4_r} + \frac{\partial}{\partial r}$$

For each of the properties, then, the following equations hold:

$$\bar{u}_{4_x}\bar{f}_{4_r} + \bar{u}_{4_r} = \bar{u}_{3_x}\bar{f}_{4_r} + \bar{u}_{3_r} \tag{4.8}$$

$$\bar{v}_{4_x}\bar{f}_{4_r} + \bar{v}_{4_r} = \bar{v}_{3_x}\bar{f}_{4_r} + \bar{v}_{3_r} \tag{4.9}$$

$$\bar{p}_{4_x}\bar{f}_{4_r} + \bar{p}_{4_r} = \bar{p}_{3_x}\bar{f}_{4_r} + \bar{p}_{3_r} \tag{4.10}$$

$$\bar{T}_{4_x}\bar{f}_{4_r} + \bar{T}_{4_r} = \bar{T}_{3_x}\bar{f}_{4_r} + \bar{T}_{3_r} \tag{4.11}$$

From the conditions at the slipstream

$$\bar{p}_{4_x} + \bar{p}_{4_r}\bar{h}_x = \bar{p}_{5_x} + \bar{p}_{5_r}\bar{h}_x \tag{4.12}$$

and from the conditions of flow on either side of the slipstream

$$\bar{u}_{4_x}\bar{h}_x + \bar{u}_4\bar{h}_{xx} - \bar{v}_{4_x} + \bar{u}_{4_r}\bar{h}_x^2 - \bar{v}_{4_r}\bar{h}_x = 0 \tag{4.13}$$

$$\bar{u}_{5_x}\bar{h}_x + \bar{u}_5\bar{h}_{xx} - \bar{v}_{5_x} + \bar{u}_{5_r}\bar{h}_x^2 - \bar{v}_{5_r}\bar{h}_x = 0 \tag{4.14}$$

The remaining equations in the system are derived from the following four shock equations:

Continuity of mass

$$\bar{p}_1\bar{T}_2\bar{\varrho}_1 = \bar{p}_2\bar{T}_1\bar{\varrho}_2$$

r-Momentum

$$\left(\bar{u}_5 - \bar{u}_1\right)\bar{f}_{3_r} + \bar{v}_5 - \bar{v}_1 = 0$$

Energy

$$\left(\bar{u}_5 + \bar{u}_1\right)\left(\bar{u}_5 - \bar{u}_1\right) + \left(\bar{v}_5 + \bar{v}_1\right)\left(\bar{v}_5 - \bar{v}_1\right) + \left(\hat{w}_5 + \hat{w}_1\right)\left(\hat{w}_5 - \hat{w}_1\right) + \frac{2\gamma R\left(\bar{T}_5 - \bar{T}_1\right)}{\gamma - 1} = 0$$

Combination of all shock equations

$$2\gamma\bar{T}_1\left(1 + \bar{f}_r^2 + \frac{f_\psi^2}{r^2}\right) = (\gamma + 1)\bar{\varrho}_1\bar{\varrho}_2 - (\gamma - 1)\bar{\varrho}_1^2$$

Taking the tangential derivative of each of these equations along the resultant shock f_3 yields the following four equations:

$$\left(\bar{p}_1\bar{T}_{5_x}\bar{Q}_1 - \bar{p}_{5_x}\bar{T}_1\bar{Q}_5 - \bar{p}_5\bar{T}_1\bar{u}_{5_x} + \bar{p}_5\bar{T}_1\bar{v}_{5_x}\bar{f}_{3_r}\right)\bar{f}_{3_r}$$

$$+ \bar{p}_1\bar{T}_{5_r}\bar{Q}_1 - \bar{p}_{5_r}\bar{T}_1\bar{Q}_5 - \bar{p}_5\bar{T}_1\bar{u}_{5_r} + \bar{p}_5\bar{T}_1\bar{v}_{5_r}\bar{f}_{3_r}$$

$$+ \bar{p}_5\bar{T}_1\bar{f}_{3_{rr}} + \bar{p}_1\bar{T}_5\bar{v}_1\bar{f}_{3_{rr}} = \left(\bar{p}_5\bar{T}_{1_x}\bar{Q}_2 - \bar{p}_{1_x}\bar{T}_5\bar{Q}_1 - \bar{p}_1\bar{T}_5\bar{Q}_{1_x}\right)\bar{f}_{3_r}$$

$$+ \bar{p}_5\bar{T}_{1_r}\bar{Q}_5 - \bar{p}_{1_r}\bar{T}_5\bar{Q}_1 - \bar{p}_1\bar{T}_5\bar{u}_{1_r} + \bar{p}_1\bar{T}_5\bar{v}_{1_r}\bar{f}_{3_r} + \bar{p}_1\bar{T}_5\bar{v}_1\bar{f}_{3_{rr}} \qquad (4.15)$$

$$\left(\bar{u}_{5_x}\bar{f}_{3_r} + \bar{v}_{5_x}\right)\bar{f}_{3_r} + \bar{u}_{5_r}\bar{f}_{3_r} + \bar{u}_5\bar{f}_{3_{rr}} + \bar{v}_{5_r}$$

$$= \bar{u}_{1_x}\bar{f}^2_{3_r} + \bar{v}_{1_x}\bar{f}_{3_r} + \bar{u}_{1_r}\bar{f}_{3_r} + \bar{u}_1\bar{f}_{3_{rr}} + \bar{v}_{1_r} \qquad (4.16)$$

$$\left(\bar{u}_5\bar{u}_{5_x} - \bar{u}_1\bar{u}_{1_x} + \bar{v}_5\bar{v}_{5_x} - \bar{v}_1\bar{v}_{1_x} + \frac{\gamma}{\gamma-1}\bar{T}_{5_x} - \frac{\gamma}{\gamma-1}\bar{T}_{1_x}\right)\bar{f}_{3_r}$$

$$+ \bar{u}_5\bar{u}_{5_r} - \bar{u}_1\bar{u}_{1_r} + \bar{v}_5\bar{v}_{5_r} - \bar{v}_1\bar{v}_{1_r} + \frac{\gamma}{\gamma-1}\bar{T}_{5_r} - \frac{\gamma}{\gamma-1}\bar{T}_{1_r} = 0 \qquad (4.17)$$

$$2\gamma\left[\left(\bar{T}_{1_x}\bar{f}_{3_r} + \bar{T}_{1_r}\right)\left(1 + \bar{f}^2_{3_r}\right) + 2\bar{T}_1\bar{f}_{3_r}\bar{f}_{3_{rr}}\right] = \left[(\gamma+1)\left(\bar{Q}_{1_x}\bar{Q}_5\right.\right.$$

$$\left. + \bar{Q}_1\bar{u}_{5_x} - \bar{Q}_1\bar{v}_{5_x}\bar{f}_{3_r}\right) - (\gamma-1)\,2\bar{Q}_1\bar{Q}_{1_x}\Big]\bar{f}_{3_r} + \Big[(\gamma+1)\left(\bar{u}_{1_r}\bar{Q}_5\right.$$

$$\left. - \bar{v}_{1_r}\bar{Q}_5\bar{f}_{3_r} - \bar{Q}_5\bar{v}_1\bar{f}_{3_{rr}} + \bar{Q}_1\bar{u}_{5_r} - \bar{Q}_1\bar{v}_{5_r}\bar{f}_{3_r} - \bar{Q}_1\bar{v}_5\bar{f}_{3_{rr}}\right)$$

$$- (\gamma-1)\,2\bar{Q}_1\left(\bar{u}_{1_r} - \bar{v}_{1_r}\bar{f}_{3_r} - \bar{v}_1\bar{f}_{3_{rr}}\right)\Big] \qquad (4.18)$$

If it is assumed that all quantities in regions 1 and 3 are known, then the unknowns in the system are $\bar{u}_{4_x}$, $\bar{v}_{4_x}$, $\bar{p}_{4_x}$, $\bar{T}_{4_x}$, $\bar{u}_{4_r}$, $\bar{v}_{4_r}$, $\bar{p}_{4_r}$, $\bar{T}_{4_r}$, $\bar{u}_{5_x}$, $\bar{v}_{5_x}$, $\bar{p}_{5_x}$, $\bar{T}_{5_x}$, $\bar{u}_{5_r}$, $\bar{v}_{5_r}$, $\bar{p}_{5_r}$, $\bar{T}_{5_r}$, the curvature of the slipstream h_{xx}, and the curvature of the resultant shock $f_{3_{rr}}$. This system of 18 linear equations is closed and has 18 unknowns. A matrix solution of this system yields the needed spatial derivatives for the system of equations (3.24) to (3.47).

4.2 Spatial Derivatives in Regions 1 and 3

For the spatial derivatives in regions 4 and 5 to be found, it is necessary that they be known in regions 1 and 3. By the use of characteristic equations and some difference methods, some of these have already been calculated in the MMOC program. In region 1, already available are $\bar{u}_x$, $\bar{v}_x$, and $\bar{s}_x$.

Once it has been determined that an intersection occurs before the next C^- characteristic, then the characteristic subroutine is called as if the shock were not there. Data points 1 and 3 (see sketch F) are used to calculate the location of

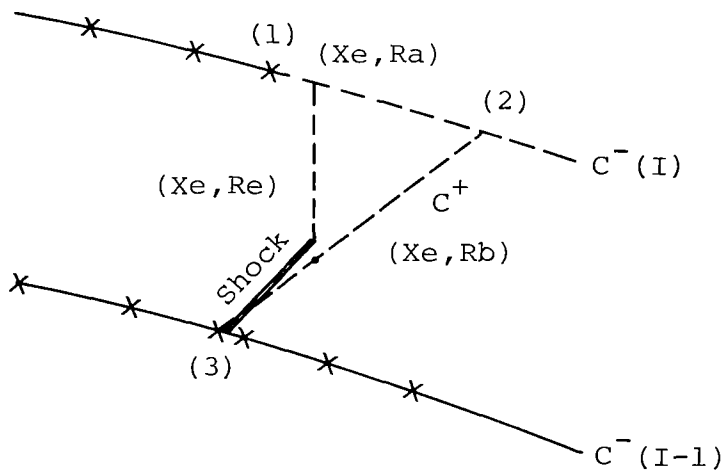

Sketch F

point 2 and all variables at point 2. A straight line interpolation is made along C^- between points 1 and 2 to get all values at Xe on that characteristic. Another interpolation is made along C^+ between points 2 and 3 to get values along this characteristic at Xe. Values at (Xe,Re) ahead of the first shock are then found by interpolating between Ra and Rb to get values at Re. Values of $\bar{u}_r$ and $\bar{v}_r$ are estimated in region 1 at (Xe,Re) by a simple difference equation between Ra and Rb.

$$\bar{u}_r = \frac{ua - ub}{Ra - Rb} \tag{4.19}$$

$$\bar{v}_r = \frac{va - vb}{Ra - Rb} \tag{4.20}$$

With these values of $\bar{u}_r$ and $\bar{v}_r$ and the values of $\bar{u}_x$, $\bar{v}_x$, and $\bar{S}_x$ already provided by the characteristic program, other spatial derivatives in region 1 are calculated in the following manner. From the x-momentum equation,

$$\bar{p}_{1_x} = \frac{1}{\bar{T}_1}\left(-\bar{p}_1\bar{u}_1\bar{u}_{1_x} - \bar{p}_1\bar{v}_1\bar{u}_{1_r}\right) \tag{4.21}$$

From the entropy equation,

$$T_{1_x} = \frac{(\gamma - 1)\bar{T}_1}{\gamma}\left(\bar{S}_{1_x} + \frac{\bar{p}_{1_x}}{\bar{p}_1}\right) \tag{4.22}$$

From the r-momentum equation,

$$\bar{p}_{1_r} = \frac{1}{R\bar{T}_1}\left(-\bar{g}\bar{p}_1 - \bar{p}_1\bar{u}_1\bar{v}_{1_x} - \bar{p}_1\bar{v}_1\bar{v}_{1_r}\right) \tag{4.23}$$

and from the continuity equation,

$$\bar{T}_{1_r} = \frac{1}{\bar{p}_1\bar{v}_1}\left(\bar{T}_1\bar{p}_1\bar{u}_{1_x} + \bar{T}_1\bar{p}_1\bar{v}_{1_r} + \frac{\bar{T}_1\bar{p}_1\hat{w}_1}{r} + \bar{u}_1\bar{T}_1\bar{p}_{1_x}\right.$$

$$\left. + \bar{v}_1\bar{T}_1\bar{p}_{1_r} - \bar{u}_1\bar{p}_1\bar{T}_{1_x} + \frac{\bar{T}_1\bar{p}_1\bar{v}_1}{r}\right) \tag{4.24}$$

Equations (4.21) to (4.24) along with the derivatives already provided define all spatial derivatives needed in region 1 to determine the solution in regions 4 and 5.

The spatial derivatives $\bar{u}_x$, $\bar{u}_r$, $\bar{v}_x$, $\bar{p}_x$, $\bar{p}_r$, $\bar{T}_x$, and $\bar{T}_r$ are also needed in region 3 to provide information for the solution in regions 4 and 5. The values for $\bar{u}_x$, $\bar{u}_r$, $\bar{v}_x$, $\bar{v}_r$, and $\bar{S}_x$ are provided by the MMOC program using the characteristic equations behind the second shock. (See sketch G.)

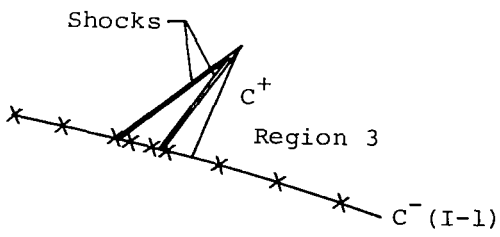

Sketch G

Again, the flow equations are used to provide the additional spatial derivatives needed in region 3

x-Momentum

$$\bar{p}_{3_x} = \frac{1}{\bar{T}_3}\left(-\bar{p}_3\bar{u}_3\bar{u}_{3_x} - \bar{p}_3\bar{v}_3\bar{u}_{3_r}\right) \tag{4.25}$$

r-Momentum

$$\bar{p}_{3_r} = \frac{1}{R\bar{T}_3}\left(-\bar{g}\bar{p}_3 - \bar{p}_3\bar{u}_3\bar{v}_{3_x} - \bar{p}_3\bar{v}_3\bar{v}_{3_r}\right) \tag{4.26}$$

Entropy

$$\bar{T}_{3_x} = \frac{(\gamma + 1)\bar{T}_3}{\gamma}\left(\bar{s}_{3_x} + \frac{\bar{p}_{3_x}}{\bar{p}_3}\right) \tag{4.27}$$

Continuity

$$\bar{T}_{3_r} = \frac{1}{p_3 v_3}\left(\bar{T}_3\bar{p}_3\bar{u}_{3_x} + \bar{T}_3\bar{p}_3\bar{v}_{3_r} + \frac{\bar{T}_3\bar{p}_3\hat{w}_3}{r}\right.$$

$$\left. + \bar{u}_3\bar{T}_3\bar{p}_{3_x} + \bar{v}_3\bar{T}_3\bar{p}_{3_r} - \bar{u}_3\bar{p}_3\bar{T}_{3_x} + \frac{\bar{T}_3\bar{p}_3\bar{v}_3}{r}\right) \tag{4.28}$$

Equations (4.25) to (4.28) and the derivatives provided by the characteristics in the MMOC program are used to determine the required spatial derivatives in region 3. There is now sufficient information available for the linear system in regions 4 and 5 to define all 16 spatial derivatives needed there.

5. PROCEDURE FOR COMBINING COALESCENCE WITH MMOC PROGRAM

5.1 Establishing Point of Coalescence

In the MMOC program, calculations are performed from the bow shock along the C^- characteristic until either the last data point on the previous characteristic is reached or until the initial data line is intersected. (See sketch H.) The embedded shocks are either included as input, or else they occur during computation when characteristics of the same family cross each other. The program keeps track of the location of each embedded shock, and when each is reached, a separate routine is used to calculate the solution. The embedded shock routine uses the shock equations and the compatibility equation along the C^+ characteristic from the previous C^-

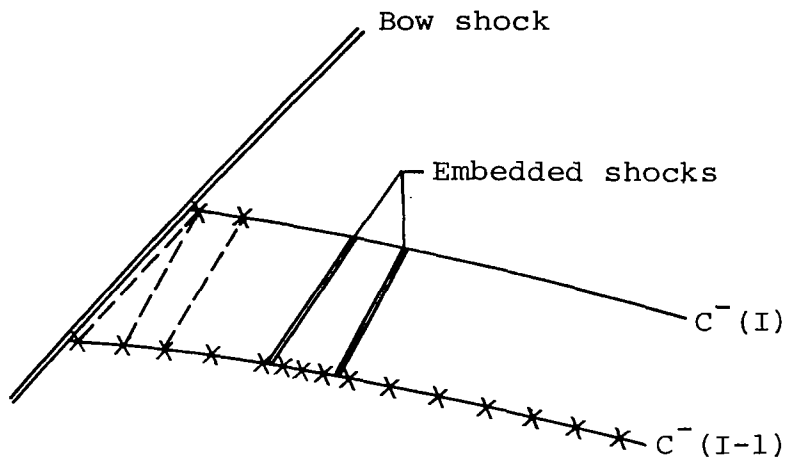

Sketch H

characteristic to determine the solution just behind the shock. (See sketch I.) These equations determine the shock position, slope, curvature, and all variables behind the shock.

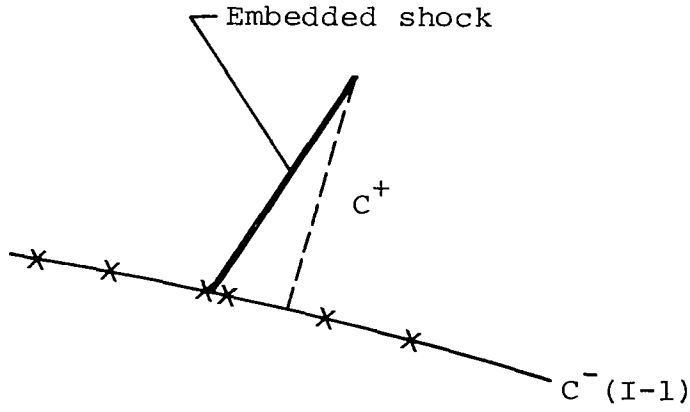

Sketch I

The program monitors the location of all shocks, and when they are close to each other, a test is made to see if they cross each other before the next characteristic line. This test involves a straight line extrapolation of both shocks to estimate their intersection point Xe and an estimate of the point XI at which the first shock crosses the next C^- characteristic as shown in sketch J. If Xe is less than XI, control is passed to the coalescence routine with all data on the I-1th characteristic known and the data at points 1, 2, and 3 held.

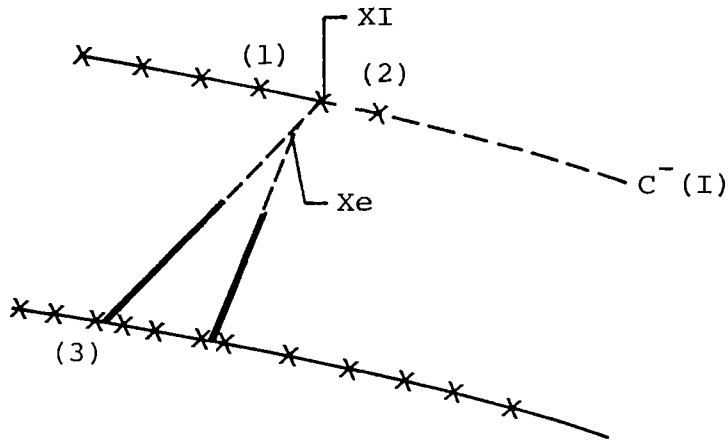

Sketch J

The following steps are then taken to determine the intersection point (Xe,Re) (see sketch K):

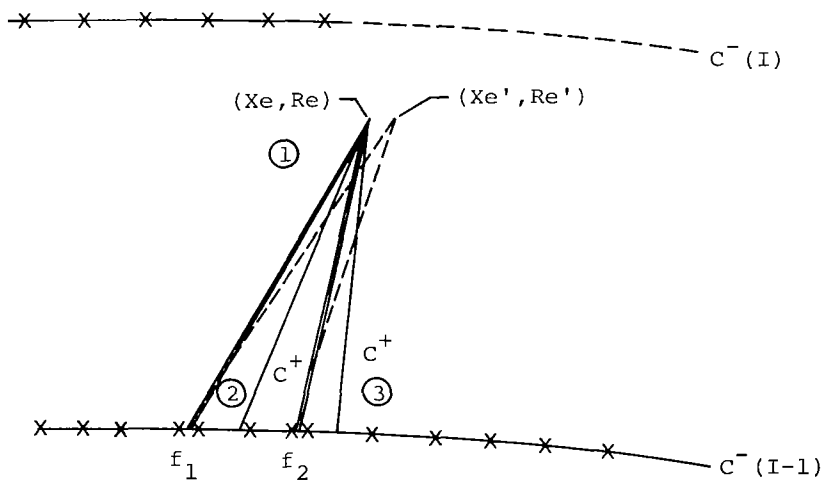

Sketch K

(1) Interpolate between data points 1, 2, and 3 to get values for all variables just ahead of the estimated intersection point in region 1.

(2) Use the results of step 1 as data just ahead of the shock. Call the subroutine of the MMOC program which finds embedded shock solutions. This subroutine gives a local value of β_1' at Xe and the values of all the variables just behind the first shock.

(3) Take the values of all variables behind shock 1 as the values in front of shock 2. Call the embedded shock subroutine to get the shock solution. This gives a value of β_2' and the values of all variables in region 3 at the intersection point.

(4) Adjust β_1 by taking $\beta_{1,new} = \left(\beta_1 + \beta_1'\right)/2$ and $\beta_{2,new} = \left(\beta_2 + \beta_2'\right)/2$. Calculate a new value of (Xe,Re) using the adjusted values of β_1 and β_2.

(5) Repeat steps 1 to 4 until the adjusted values of β_{new} change less than some error criterion ε. Generally it is found that only three or four iterations are necessary with the error criterion on the order of 10^{-10}.

When the above iteration has converged, the location of the coalescence point (Xe,Re) has been determined. Also known are the values of the variables in regions 1 and 3, the local shock angles β_1 and β_2, and the local curvatures $\tilde{f}_1$ and $\tilde{f}_2$ at the intersection point.

5.2 Local Solution

Since the point of intersection and the data immediately ahead of this point are known, the spatial derivatives in regions 1 and 3 can now be found by the method described in section 4.2. The axisymmetric solution described in section 3.1 is now performed. This solution provides values for the variables $\bar{u}$, $\bar{v}$, $\bar{p}$, $\bar{T}$, and $\bar{S}$ in regions 4 and 5. It also provides the local slopes of f_3, f_4, and the slope of the slipstream h. The axisymmetric solution is independent of any of the tilde variables and $\hat{w}$, and is found without iteration once the position of intersection is solved. The linear system described in section 4.1 is solved for the spatial derivatives of the variables in regions 4 and 5. There is now sufficient information to perform the asymmetric solution as described in section 3.2. This solution provides the values for $\tilde{u}$, $\tilde{v}$, $\tilde{p}$, $\tilde{T}$, and $\tilde{S}$ in regions 4 and 5 for $\tilde{h}_x$, $\tilde{h}$, $\tilde{f}_3$, $\tilde{f}_4$, and $\tilde{f}_{3_r}$. The local solution is now complete.

5.3 Incorporation of Solution into Characteristic Network

The resultant shock f_3 is extrapolated linearly upward to obtain a first approximation of its intersection point with the Ith C^- characteristic, as shown in sketch L. Data at points 1 and 2 are known from the calculation described in

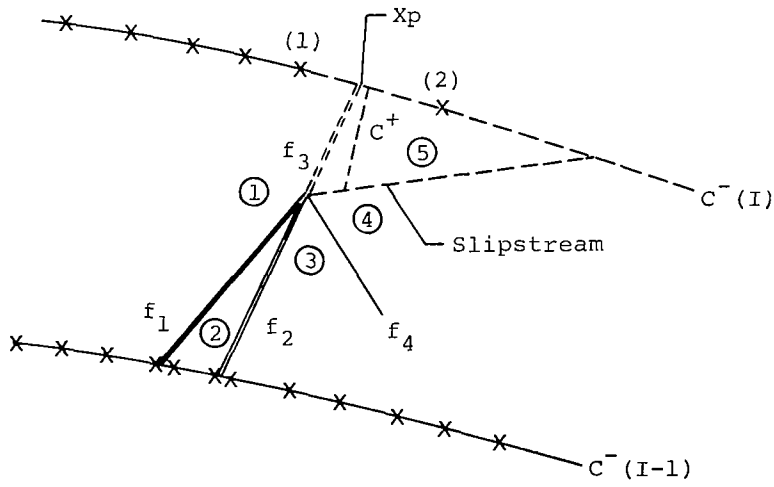

Sketch L

section 5.1. A linear interpolation is used to find the value of all variables ahead of Xp, the intersection point. From the shock equations, the data ahead of the shock at Xp, and the C^+ characteristic running from behind the shock at Xp to the top of the slipstream, a solution is found for β_3' at Xp. $\beta_{3,new}$ is calculated using $(\beta_3 + \beta_3')/2$, and the process is repeated until $\beta_{3,new}$ does not change between iterations.

The point Xp and the data immediately behind the shock at Xp have now been determined. To retain the effects of the data below the slipstream, a new C^- characteristic (see sketch M) is calculated from the intersection point (Xe,Re) using the data from region 4. The characteristic subroutine is called with data at points 1

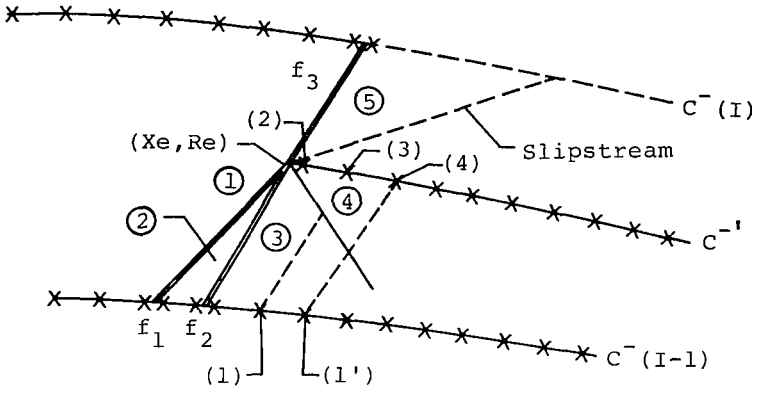

Sketch M

and 2 to calculate point 3, at points 1' and 3 to calculate point 4, and so on, until the end of the data on the I-1th characteristic is reached.

At this point, it is recognized that the difference in entropy across the slipstream is extremely small. It is convenient, therefore, to disregard the actual location of the slipstream and to allow the tangential discontinuity to become smeared in the region between C^-' and f_3. The remainder of the Ith characteristic is now calculated using data from the intermediate characteristic C^-'. The effects of the data above the slipstream are felt in the location of Xp and in the data immediately behind Xp. (See sketch N.) The effects of the data below the slipstream appear

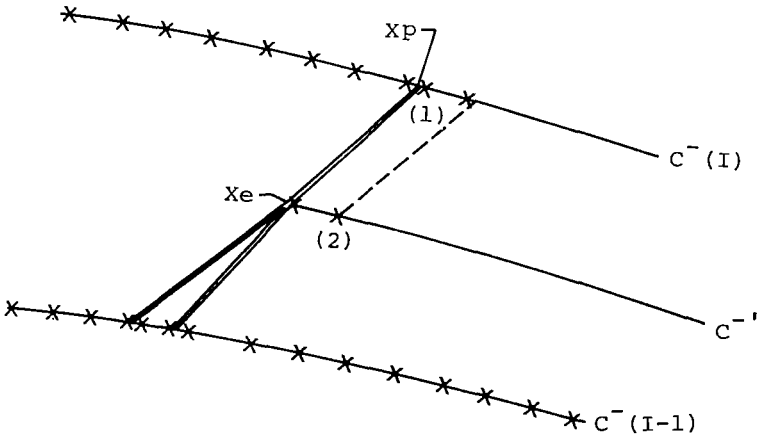

Sketch N

in the value of the variables on the C^- characteristic. To complete the Ith characteristic, the characteristic subroutine is called using points 1 and 2 to calculate point 3, and so on, until the characteristic is completed. Control of the program now reverts from the shock coalescence routine to the main program. If, instead of two embedded shocks intersecting, the bow shock intersects an embedded shock, the same procedure is followed with simplifications made because of the constant values ahead of the bow shock.

6. RESULTS AND DISCUSSION

The MMOC is a propagation method rather than a prediction method. Thus, flow-field input data on a cylindrical surface at approximately one body length from the axis must be supplied either from experiment or by use of computational methods. To employ the MMOC in an axisymmetric case, the initial data must include x, r, θ, M, z_∞, and S/R at points on the cylinder in the plane $\psi = 0$. In addition, the strength of the bow shock and the location and strength of any embedded shocks must be given. For asymmetric cases, u, v, w, and S/R are also required.

At the outset of the current work, it was felt that the flow-field computational method described in reference 25 represented the most accurate means available for predicting the data required as input to the MMOC. There also exist two alternate methods which can be used to calculate the field in the vicinity of the body, and both of these are also able to handle shock coalescence if they are allowed to calculate to the far field. The first, referred to as the modified uniform atmosphere method (MUAM), is described in reference 26. In this method, based on Whitham theory, a uniform atmosphere is assumed, and a geometric mean correction for ambient pressure $\sqrt{p_a p_g}$ (where p_a is the pressure at the calculation altitude, and p_g is the ground pressure) is employed. In the second method, denoted as ARAP, geometric acoustics theory is used, and variable density in the atmosphere is accounted for. Each of these methods requires as input a description of the body and the flight conditions (ref. 27).

Since the axisymmetric shock coalescence is a new feature of the MMOC, it was initially decided to exercise this version of the program. Input data were provided for the MMOC at $d/\ell = 0.2$ by the method of reference 25 on a body of revolution to compare the extrapolated results of the MMOC with results predicted by the MUAM and ARAP programs. These axisymmetric results are discussed later in this section.

The same body of revolution was placed at a small, positive angle of attack in order to obtain nonaxisymmetric data, and the method of reference 25 again was applied to calculate the required quantities at $d/\ell = 0.2$. At this point, two difficulties arose which ultimately led to a decision to abandon the method of reference 25 in favor of a less expensive, and presumably somewhat less accurate, determination of the required data. First, the scheme of reference 25 is used to calculate quantities on a cylinder coaxial with the body and not on constant r, as required in the current work. Second, the presence of cross-derivative terms proportional to $1/r$ throughout the asymmetric version of MMOC equations gives rise to numerical difficulties unless the initial surface is at least one body length away from the axis, a distance which requires excessive computation time when the method of reference 25 is used for flow Mach numbers of 3 or 4. Since the aim of the current numerical computations was only to demonstrate the results of the new analysis, it was felt that continued use of this method for obtaining input data was not justified. Rather, it was decided to make use of the MUAM to determine appropriate data as input to the MMOC. The MUAM was modified to calculate cross-flow components, and the

derivatives with respect to ϕ needed as input to the MMOC were calculated from their analytical expressions in the MUAM program. Accordingly, figure 1 includes the body used and the results obtained with the method of reference 25 for the axisymmetric case. All other results were obtained using a different body, and the MUAM was used to provide initial data for the MMOC at $d/\ell = 1.0$.

Axisymmetric data for the body of revolution shown in figure 1 were obtained using the method of reference 25 on a cylindrical surface at $d/\ell = 0.2$. The pressure signature in the plane $\phi = 0$ at this radial location is shown. The MMOC program was then used to extrapolate this field through 900 body lengths to the ground. The resulting pressure signature is illustrated at the bottom of figure 1. It is emphasized that the evolution of the signature in figure 1 involves the coalescence of three shocks. Thus, even though it represents an axisymmetric case, this result cannot be obtained by using the MMOC without the analysis reported in the current paper. No comparison of this result with predictions of the MUAM or the ARAP programs was made, since it was found that these methods had difficulty converging to a solution at 0.2 body lengths from the body.

Correlations of MUAM and ARAP results with experimental data are shown in figures 2 to 4. Figure 2 shows a comparison made in reference 26 for a body of revolution at an angle of attack of 0° and a Mach number of 2.96. Though the bow shock amplitude is not predicted accurately, the expansion and tail pressures are well defined by the MUAM. Figure 3 shows a comparison of MUAM results with experimental data from reference 28. These data include angles of attack of 3° and -3° at Mach numbers of 1.41 and 2.01. The data points were read with pressure orifices on a reflection plate, and thus, a reflection factor of 2 has been used in the MUAM results. The experimental data show some scatter in these figures, but the pressure levels and trends are still rather well predicted by the MUAM at these distances for all angles of attack shown. No pressure data were available to verify pressures from the MUAM at an azimuthal angle other than $\phi = 0$.

A correlation of flight-test data with ARAP predictions was made in reference 7. Figure 4 is a reproduction of one such correlation made for Mach numbers of 1.35 to 3.00 over an altitude ranging from 35 000 feet to 70 000 feet. This figure shows that both the amplitude and the duration of the flight-test signatures were well predicted by the ARAP program.

As originally written, the ARAP program was a sonic boom propagation method which required the Whitham F function as input. It was later modified to accept an area distribution which was transformed to the Whitham F function. This modification is based on having a smooth body with no discontinuities in slope. Though restricted to bodies of revolution, the MUAM program is not limited to smooth bodies. A second difference between the MUAM and the ARAP programs is that signals begin from the axis in the ARAP program and from the body surface in the MUAM program. Thus, when discontinuities are present, near-field shocks are more accurately located by the MUAM.

With the experimental data shown then, it is felt that confidence can be placed in the pressure signature predictions by the MUAM in the near field for a body of revolution and in the ground level predictions made by the ARAP. Because there are no experimental data by which we can verify the results of the MMOC, comparisons are made of the MMOC results and the MUAM and ARAP results. Results from the MUAM at one body length were used to provide initial data for the MMOC. Comparisons of all three methods at several intermediate steps of propagation are shown.

The cone of revolution shown in figure 5 was used for the rest of the results. It has slope discontinuities at two locations so that embedded shocks are formed immediately, and thus, the shock coalescence portion of the program will be exercised. The pressure fields at one body length predicted by the MUAM and the ARAP for $M = 3.00$, $\alpha = 0°$ are shown at the upper left of figure 6.

The two signatures are quite dissimilar. Recall that it is the MUAM signature which is felt to be valid in the near field and which is, therefore, used to initialize the MMOC. The remaining portions of figure 6 show comparisons of signatures predicted by all three methods during propagation. Note that at this Mach number and angle of attack, the MMOC and MUAM signatures remain very near each other through 100 body lengths. At ground level, the bow shock predictions of the MMOC and the ARAP are very near each other, although the MMOC signature is predicted to be significantly shorter. The positive and negative areas for the MMOC signature do not appear balanced in the ground signature in figure 6. However, the wave has been truncated, and considerable negative area has not been included.

Asymmetric lifting forces are added through an angle of attack of 3° in figure 7. Again, note that the MMOC and MUAM predictions remain very near each other in the near field (out to two body lengths), with the ARAP signature again being totally different. In the far-field and ground signatures, however, the shock amplitudes of the MMOC and ARAP results are very nearly equal, and the overall lengths of the signatures are not very different.

It is noted here that comparisons are made of the shape and duration of the signature and not of its location in the atmosphere as denoted by the starting location x_o. The three different methods of propagation do follow different paths through the atmosphere as determined by the position of x_o. By observing the locations shown in figure 7, note that shock coalescence of the embedded and bow shocks has occurred between 2 and 10 body lengths. The ground signatures shown in these results all include a reflection factor of 1.8.

In figure 8, even more asymmetries have been added to the flow field by increasing the angle of attack to 7°. The same general trend is seen in the near-field signatures. The difference in coalescence rate of the three methods can be observed in this figure. At two body lengths, the embedded shocks have coalesced in the MMOC and MUAM signatures but not in the ARAP signature, and at two and one-half body lengths, all shocks have coalesced in the MUAM and MMOC signatures. The ground signature again shows good correlation between the bow shock level of all signatures but at this angle of attack, the MMOC signature is now the longest of the three.

Figures 9 and 10 show a similar set of comparisons at $\alpha = 0°$ and Mach numbers of 3.50 and 4.00, respectively. At $M = 3.50$, the MMOC and ARAP ground signatures have the same bow shock level, but the MMOC signature is somewhat shorter. At $M = 4.00$, the MMOC and ARAP ground signatures are practically identical in both amplitude and length. In both figures, the MUAM ground signature predicts the lowest bow shock and the longest signature.

The experimental comparisons shown earlier for the MUAM and ARAP predictions indicate that confidence can be placed in the MUAM near-field predictions and in the ground-level ARAP predictions. These predictions are made based on a description of the equivalent body of revolution and on the flight conditions. The results from the MMOC program, when initialized with near-field MUAM data, approach ARAP ground shock predictions for all cases shown and have nearly the same signature as the ARAP at $M = 4.00$.

The fact that the MMOC program is shown to begin with valid data in the near field and to extrapolate to valid data (by comparison with the ARAP results) in the far field makes this a powerful tool in experimental work where predictions are made by the extrapolation of near-field signals. The MMOC program is also able to make sonic boom predictions for complex three-dimensional bodies when their flow fields are provided by other computational methods.

A comparison of the ground signatures when the MMOC program is initialized at two and one-half body lengths and at one body length, is shown in figure 11. The signature extrapolated from two and one-half body lengths is shorter and has a lower bow shock than the signature extrapolated from one body length. This difference is to be expected because at two and one-half body lengths in figure 8, the MUAM signature is already shorter than the MMOC signature and has a somewhat lower bow shock.

The effect of asymmetries in the case with an angle of attack of 7° is seen in figure 12. The identical flow-field conditions with no asymmetric effects result in a signature whose bow shock is approximately 7 percent higher and whose length is 3 percent shorter than the signature in which the asymmetries are included.

Because one of the primary benefits in a program such as the MMOC would be for the extrapolation of wind-tunnel data to ground-level predictions, the effect of slight deviations in the determined locations of embedded shocks is an important consideration. In figure 13, the locations of the embedded shocks were perturbed about 1 percent, and the perturbed data were extrapolated to the ground. The results for the perturbed signature indicated approximately 2-percent deviation in the shock strength and in the length of the signature.

Because a method based on linear theory was used to provide the initial data in these results, it was possible to calculate the necessary cross derivatives analytically within the MUAM program. In the course of this study, however, several methods, including curve fits and finite difference approximations, were used to compute these derivatives numerically, and it was found that the MMOC program is quite sensitive to their values. Thus, when experimental data or computational results which do not include analytically determined derivatives of the flow quantities are used to provide input to the MMOC program, extreme care must be taken in determining values for the cross derivative data.

7. CONCLUDING REMARKS

A method for analyzing shock coalescence including asymmetric effects has been presented. This method is based on an extension of the axisymmetric (locally two-dimensional) solution. The asymmetric effects are introduced through an additional set of governing equations, which are derived by taking the second circumferential derivative of the standard shock equations in the plane of symmetry. This shock coalescence method is consistent with and has been combined with a nonlinear sonic boom propagation method developed at New York University (NYU). The original NYU program, based on the method of characteristics, is unable to solve shock coalescence and ceases extrapolation when shock intersection occurs. This is often the case when data are extrapolated from realistic aircraft configurations. The combined program referred to as the modified method of characteristics (MMOC) is capable of extrapolating pressure signatures which include embedded shocks from the near field (approximately one body length from the axis) of an aircraft to ground level. Initial flow-field data are required on a cylindrical surface at approximately one body length from the aircraft axis. Flow variables and their cross derivatives are then defined

in the plane of symmetry beneath the aircraft and used during the extrapolation process. The location and strengths of all shocks on the initial surface must also be included in the data.

The MMOC program is potentially extremely useful for predicting sonic booms from configurations where near-field data are provided either experimentally or from flow-field computational methods. Unlike previous extrapolation methods, the MMOC program accounts for the variation in entropy and nonlinear effects present near the aircraft and is thus able to begin extrapolation nearer to the body than the previous requirement of about three body lengths. A major benefit of this capability is that sonic boom models may now be built approximately 3 feet in length (a restriction based on tunnel size) rather than the previous 6 inches. The larger size will allow a more detailed, realistic configuration than was previously possible.

Included in the paper are extrapolated results from a body of revolution at a small, positive angle of attack. This configuration was designed so that embedded shocks would be included in the initial data and so that the MMOC solution could be compared with existing sonic boom prediction methods. Comparisons of signatures predicted by the MMOC with those predicted by two methods based on modified linear theory show good agreement in regions of propagation where the linear methods have been experimentally verified. The coalescence method as described contains weak shock/expansion approximations to determine spatial derivatives behind the wave of the opposite family, which may be needed to obtain the complete field in the vicinity of a point where shocks intersect.

Langley Research Center
National Aeronautics and Space Administration
Hampton, VA 23665
September 26, 1983

REFERENCES

1. Siclari, Michael J.: Nonlinear Analysis of Sonic Booms. Ph. D. Diss., New York Univ., Jan. 1974.

2. Ferri, Antonio; Siclari, Michael; and Ting, Lu: Sonic Boom Analysis for High Altitude Flight at High Mach Number. AIAA Paper No. 73-1034, Oct. 1973.

3. Ferri, Antonio; Ting, Lu; and Lo, R. W.: Nonlinear Sonic-Boom Propagation Including the Asymmetric Effects. AIAA J., vol. 15, no. 5, May 1977, pp. 653-658.

4. Whitham, G. B.: The Flow Pattern of a Supersonic Projectile. Commun. Pure & Appl. Math., vol. V, no. 3, Aug. 1952, pp. 301-348.

5. Walkden, F.: The Shock Pattern of a Wing-Body Combination, Far From the Flight Path. Aeronaut. Q., vol. IX, pt. 2, May 1958, pp. 164-194.

6. Hayes, Wallace D.: Linearized Supersonic Flow. Rep. No. AL-222, North American Aviation, Inc., June 18, 1947.

7. Carlson, Harry W.; and Maglieri, Domenic J.: Review of Sonic-Boom Generation Theory and Prediction Methods. J. Acoust. Soc. America, vol. 51, no. 2, pt. 3, Feb. 1972, pp. 675-685.

8. McLean, F. Edward: Some Nonasymptotic Effects on the Sonic Boom of Large Airplanes. NASA TN D-2877, 1965.

9. Hayes, Wallace D.: Brief Review of the Basic Theory. Sonic Boom Research, A. R. Seebass, ed., NASA SP-147, 1967, pp. 3-7.

10. Jones, L. B.: Lower Bounds for Sonic Bangs in the Far Field. Aeronaut. Q., vol. XVIII, pt. 1, Feb. 1967, pp. 1-21.

11. Seebass, R.: Sonic Boom Theory. J. Aircr., vol. 6, no. 3, May-June 1969, pp. 177-184.

12. Seebass, R.; and George, A. R.: Sonic-Boom Minimization. J. Acoust. Soc. America, vol. 51, no. 2, pt 3, Feb. 1972, pp. 686-694.

13. Darden, Christine M.: Minimization of Sonic-Boom Parameters in Real and Isothermal Atmospheres. NASA TN D-7842, 1975.

14. Darden, Christine M.: Sonic-Boom Minimization With Nose-Bluntness Relaxation. NASA TP-1348, 1979.

15. Mack, Robert J.; and Darden, Christine M.: Wind-Tunnel Investigation of the Validity of a Sonic-Boom-Minimization Concept. NASA TP-1421, 1979.

16. Mack, R. J.; and Darden, C. M.: Some Effects of Applying Sonic Boom Minimization to Supersonic Cruise Aircraft Design. J. Aircr., vol. 17, no. 3, Mar. 1980, pp. 182-186.

17. Sigalla, A.; Runyan, L. J.; and Kane, E. J.: The Overland Supersonic Transport With Low Sonic Boom - A Feasibility Study. Acta Aeronaut., vol. 4, no. 1/2, Jan./Feb. 1977, pp. 163-179.

18. Carlson, Harry W.; Barger, Raymond L.; and Mack, Robert J.: Application of Sonic-Boom Minimization Concepts in Supersonic Transport Design. NASA TN D-7218, 1973.

19. Ferri, Antonio; and Wang, Huai-Chu: Observations on Problems Related to Experimental Determination of Sonic Boom. Third Conference on Sonic Boom Research, Ira R. Schwartz, ed., NASA SP-255, 1971, pp. 277-284.

20. Pan, Y. S.; and Sotomayer, W. A.: Sonic Boom of Hypersonic Vehicles. AIAA J., vol. 10, no. 4, Apr. 1972, pp. 550-551.

21. Lin, C. C.; and Rubinov, S. I.: On the Flow Behind Curved Shocks. J. Math. and Phys., vol. XXVII, no. 2, July 1948, pp. 105-129.

22. Yuan, S. W.: Foundations of Fluid Mechanics. Prentice-Hall, Inc., c.1967.

23. Thompson, Philip A.: Compressible-Fluid Dynamics. McGraw-Hill, Inc., c.1972.

24. Ferri, Antonio: The Method of Characteristics. General Theory of High Speed Aerodynamics, W. R. Sears, ed., Princeton Univ. Press, 1954, pp. 583-669.

25. Marconi, Frank; Salas, Manuel; and Yaeger, Larry: Development of a Computer Code for Calculating the Steady Super/Hypersonic Inviscid Flow Around Real Configurations. Volume I - Computational Technique. NASA CR-2675, 1976.

26. Mack, Robert J.: An Improved Method for Calculating Supersonic Pressure Fields About Bodies of Revolution. NASA TN D-6508, 1971.

27. Hayes, Wallace D.; Haefeli, Rudolph C.; and Kulsrud, H. E.: Sonic Boom Propagation in a Stratified Atmosphere, With Computer Program. NASA CR-1299, 1969.

28. Gapcynski, John P.; and Carlson, Harry W.: A Pressure-Distribution Investigation of the Aerodynamic Characteristics of a Body of Revolution in the Vicinity of a Reflection Plane at Mach Numbers of 1.41 and 2.01. NACA RM L54J29, 1955.

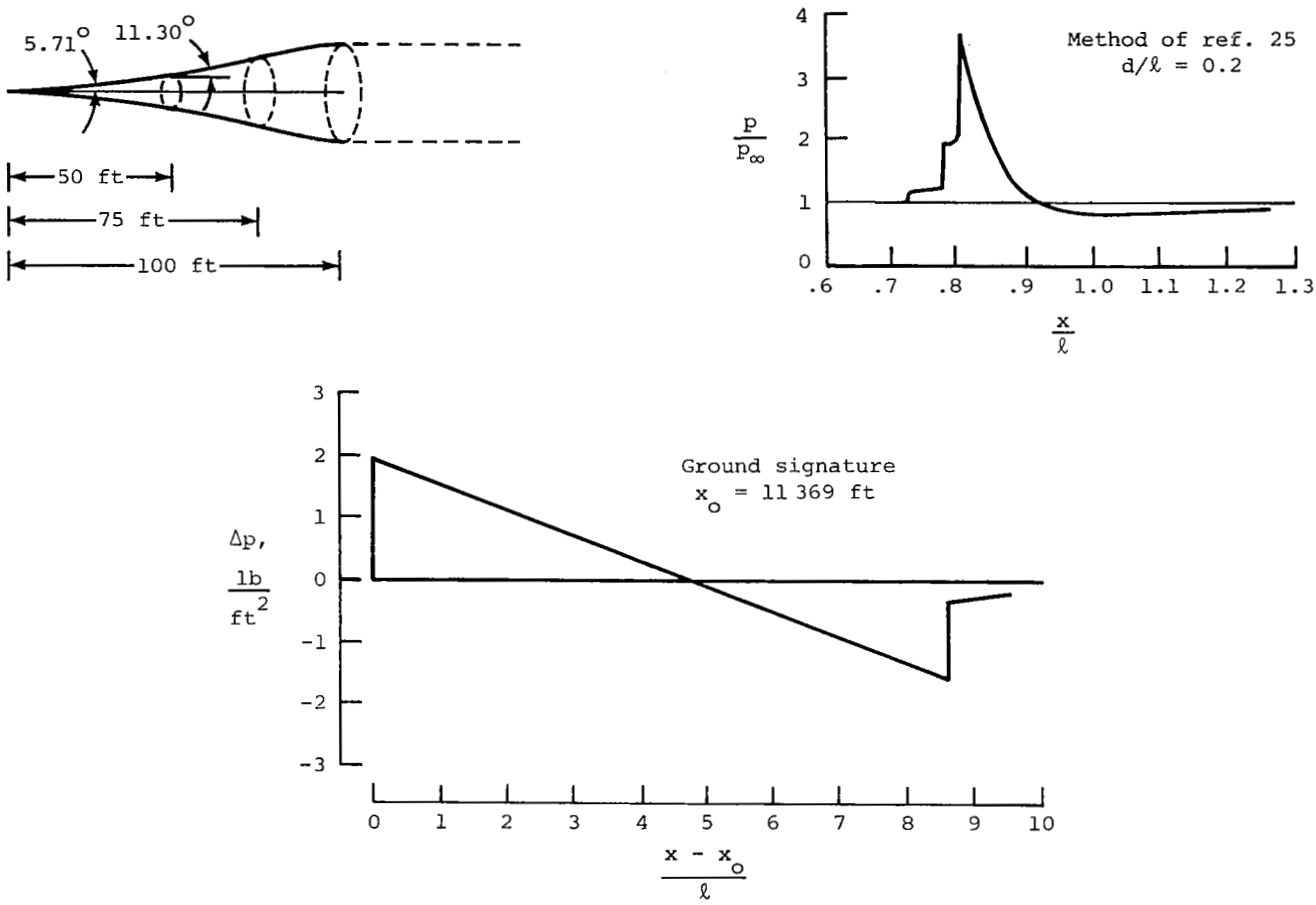

Figure 1.- Axisymmetric extrapolation using MMOC with shock coalescence. M = 4.00; alt = 90 000 ft; ℓ = 100 ft.

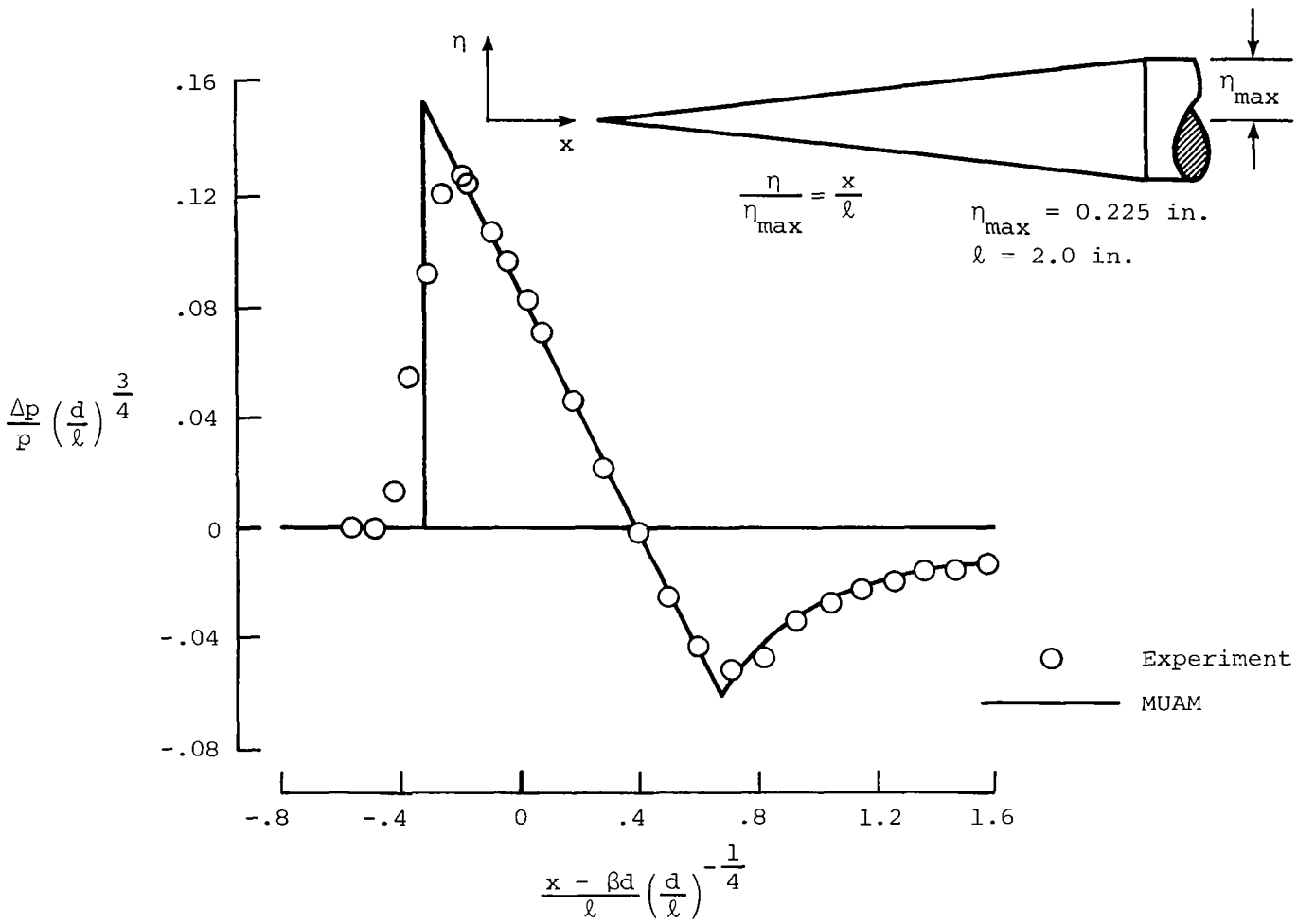

Figure 2.- Comparison of MUAM predictions and experimental data (ref. 26). M = 2.96; $d/\ell = 5.0$.

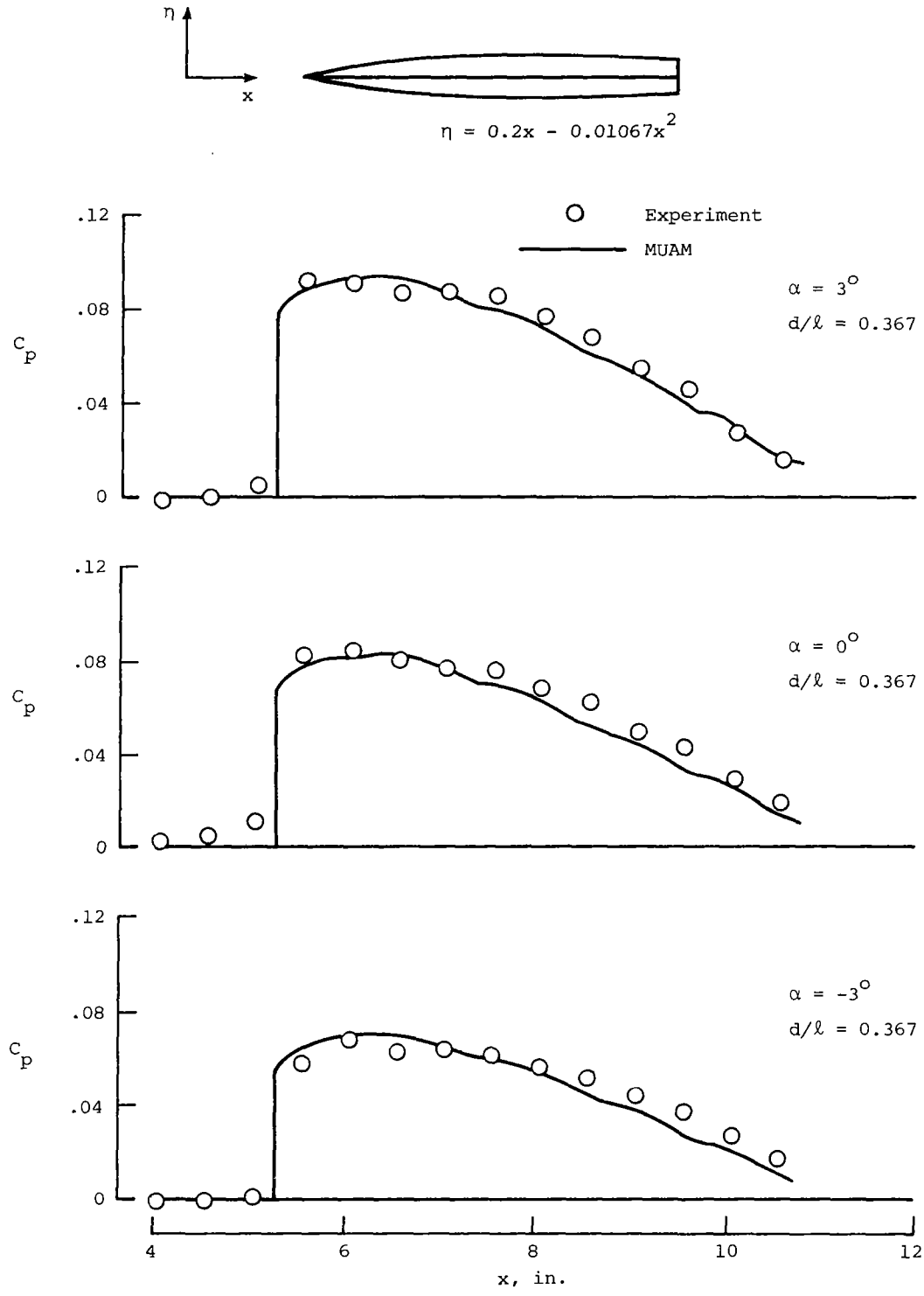

(a) M = 1.41.

Figure 3.- Comparison of MUAM predictions and experimental data (ref. 28). ℓ = 15 in.

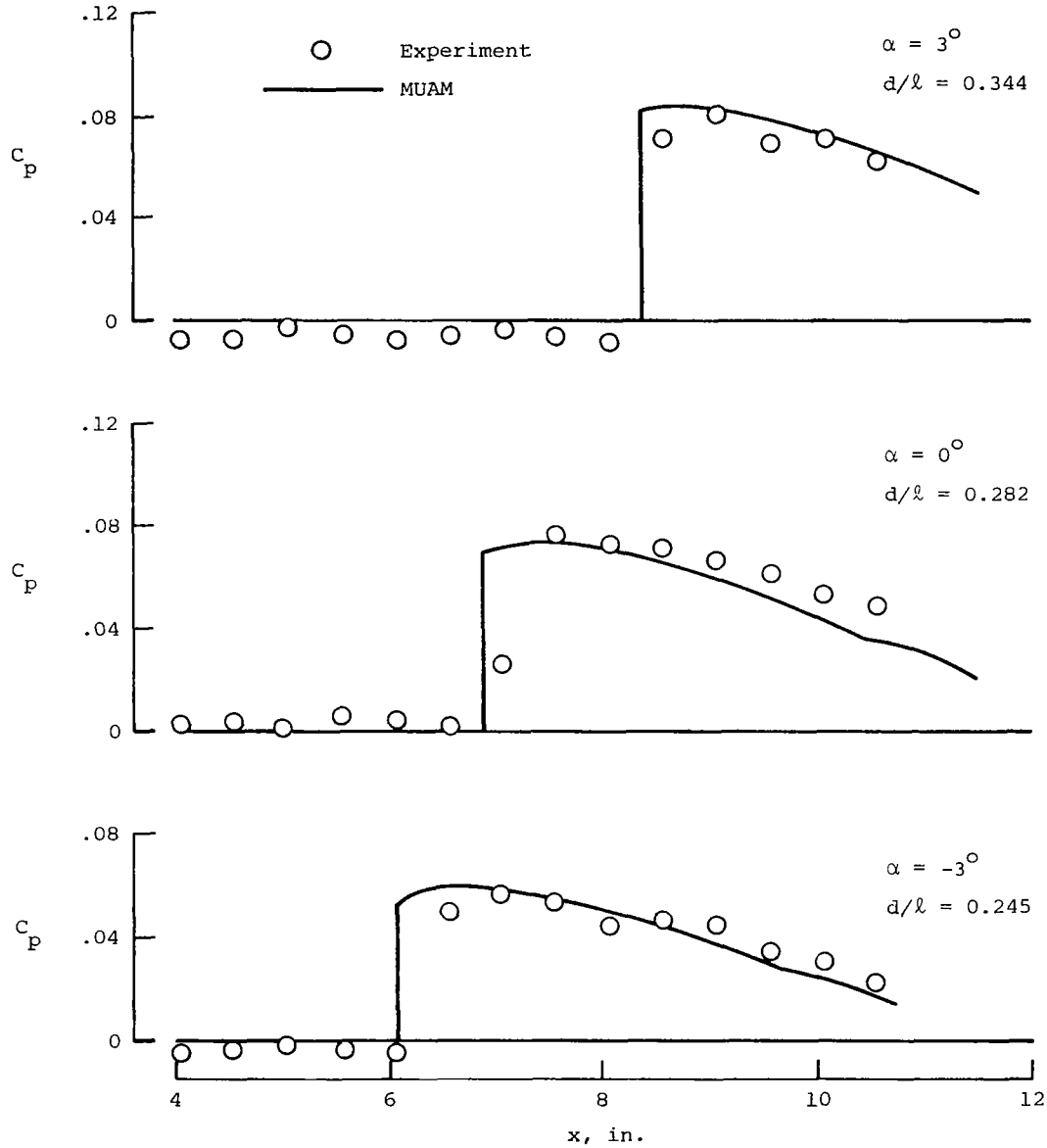

(b) M = 2.01.

Figure 3.- Concluded.

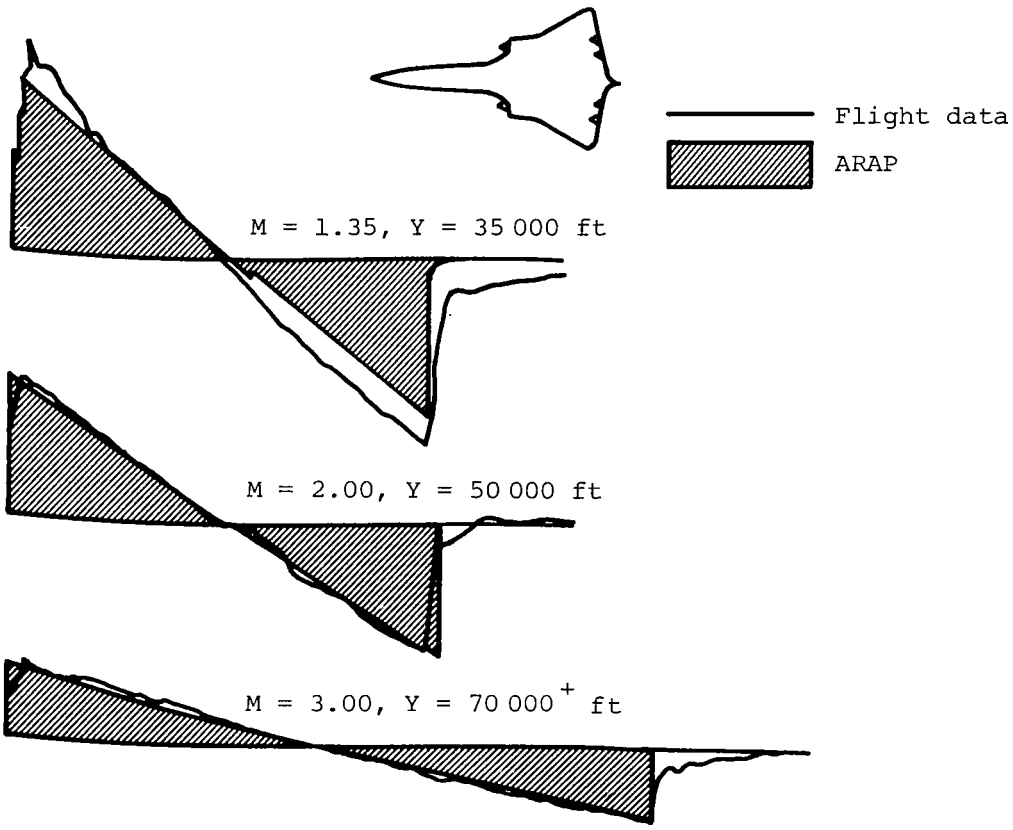

Figure 4.- Prediction of flight-test pressure signatures with ARAP (ref. 7).

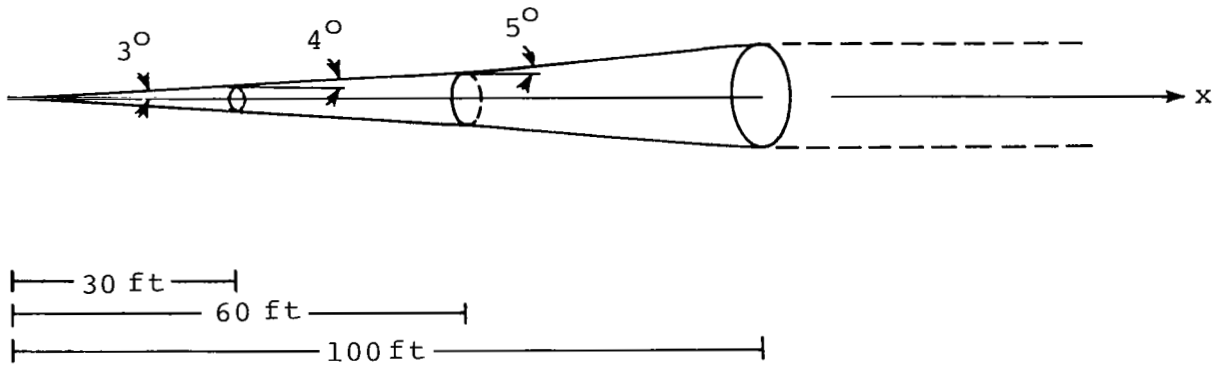

Figure 5.- Body of revolution used for comparison of MMOC with MUAM and ARAP.

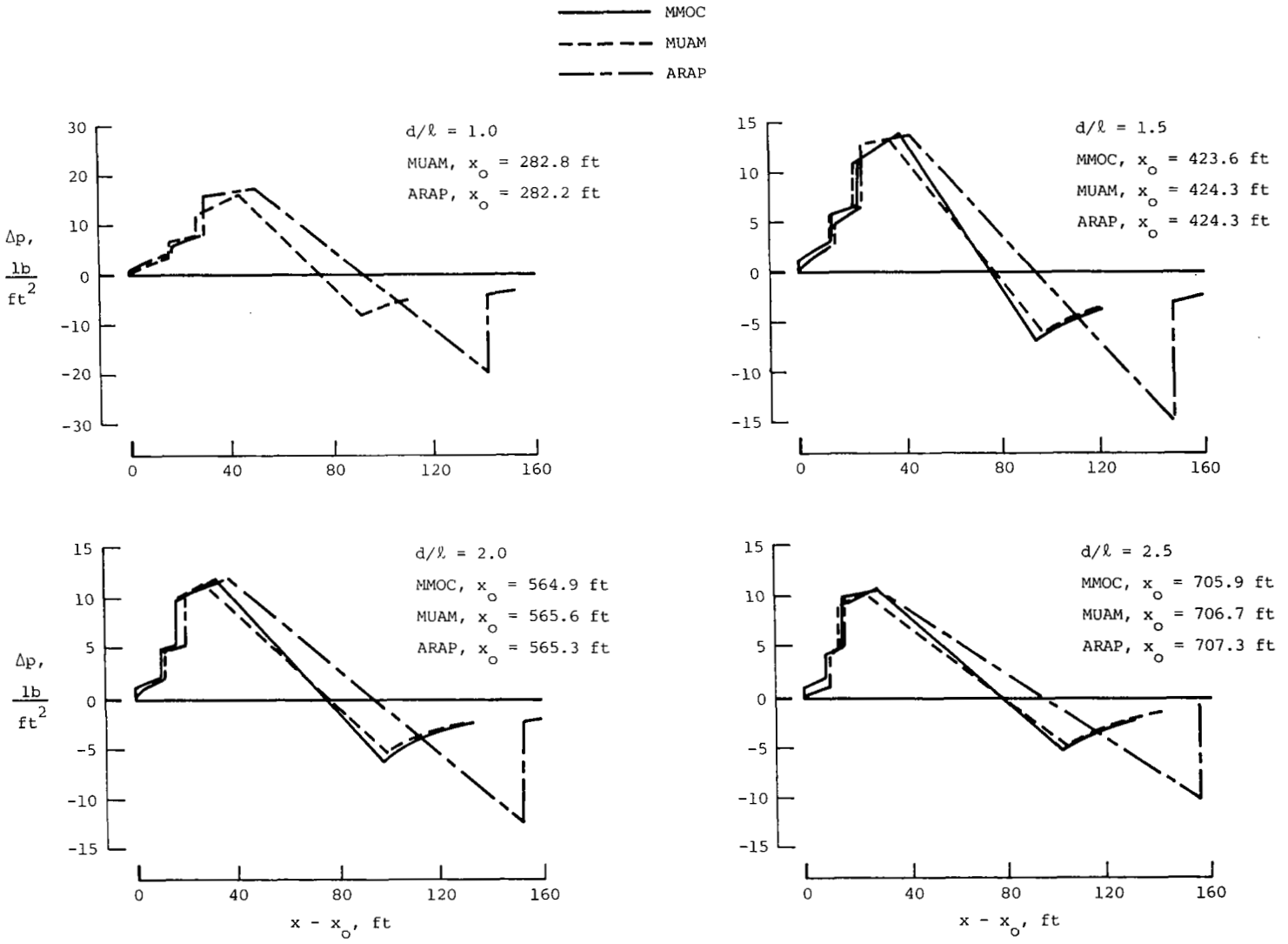

Figure 6.- Comparison of pressure signatures M = 3.00 and $\alpha = 0°$. Body of revolution, as shown in figure 5; ℓ = 100 ft; alt = 50 000 ft.

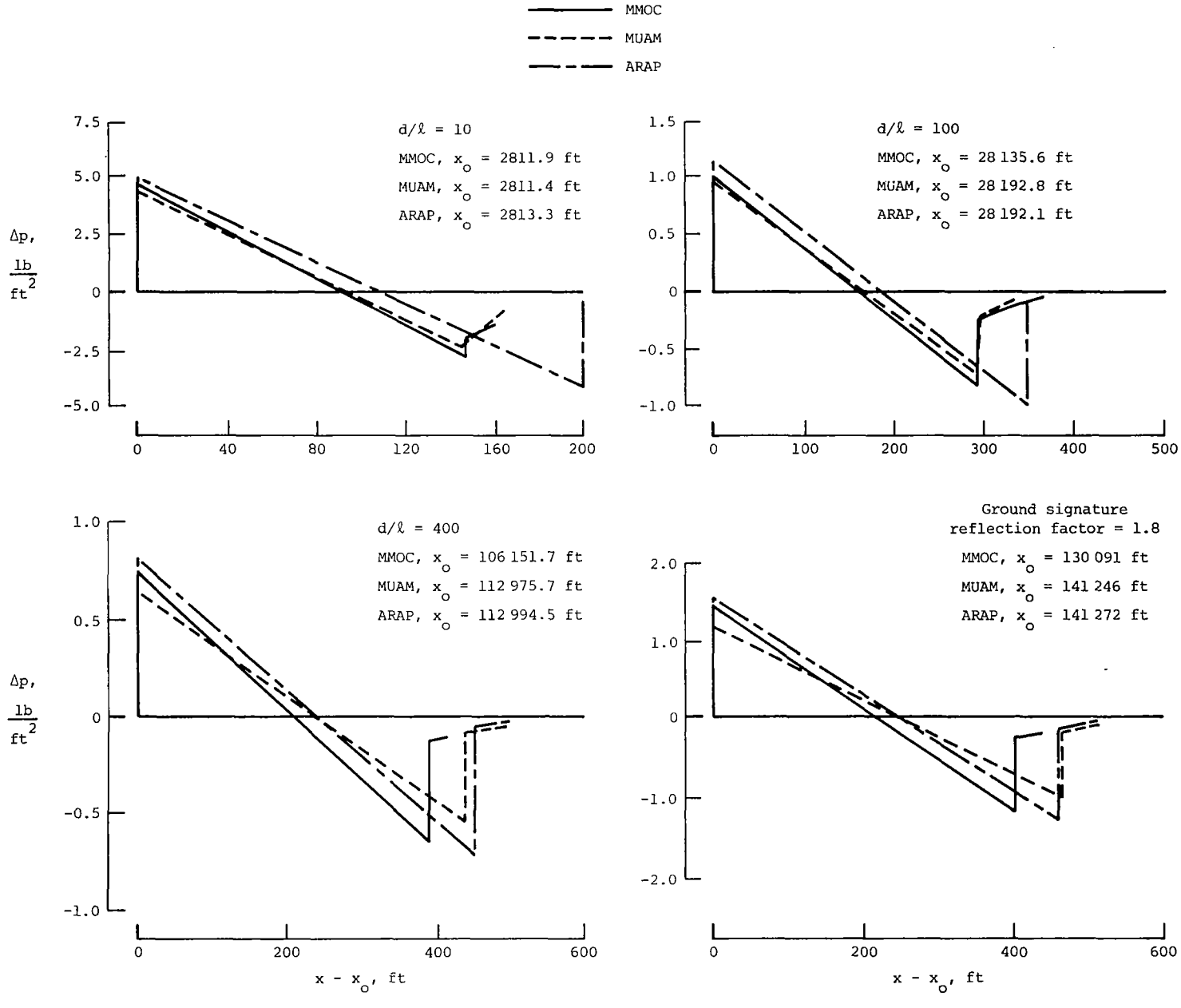

Figure 6.- Concluded.

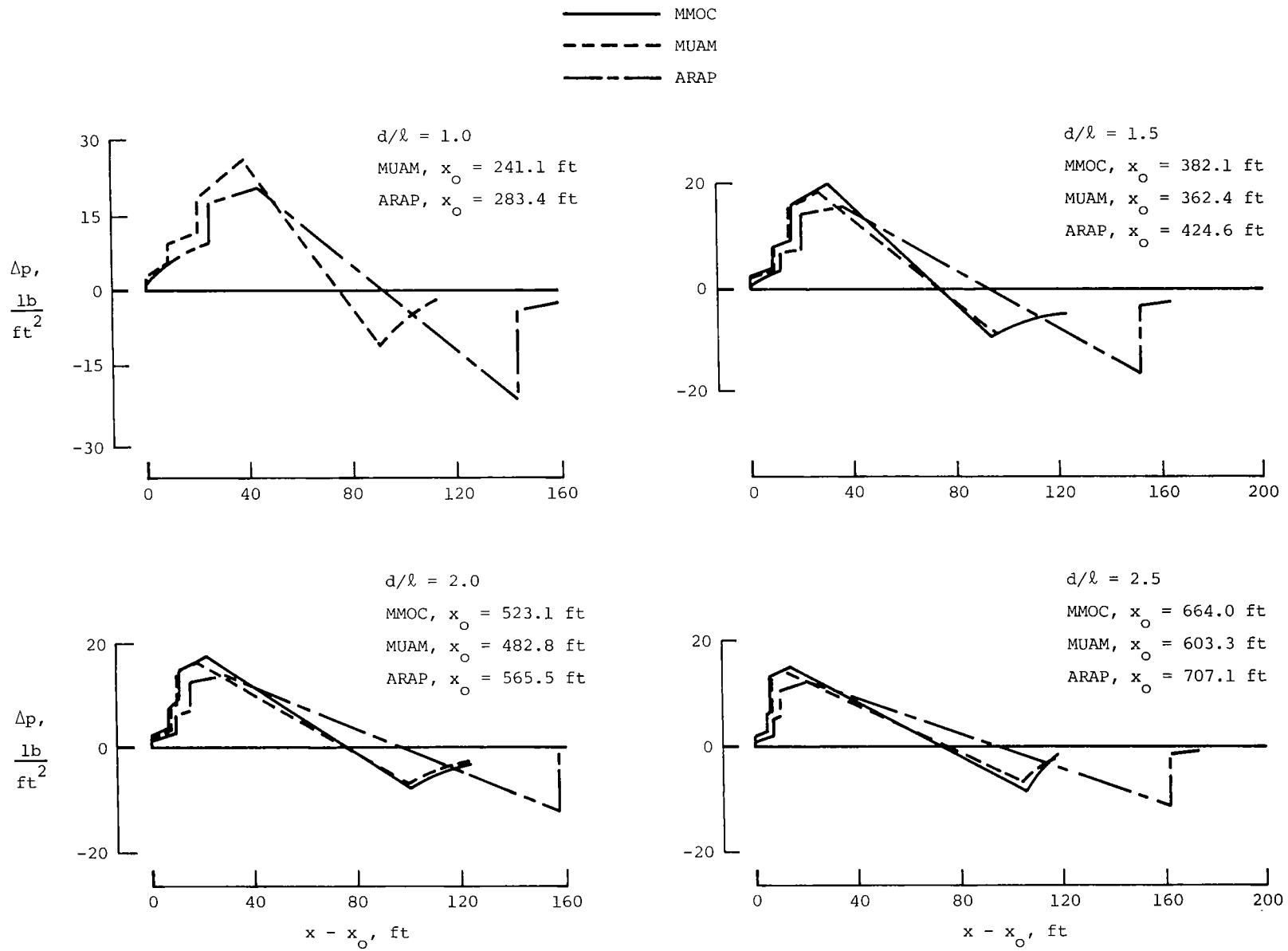

Figure 7.- Comparison of pressure signatures at M = 3.00 and $\alpha = 3°$. Body of revolution as shown in figure 5; ℓ = 100 ft; alt = 50 000 ft.

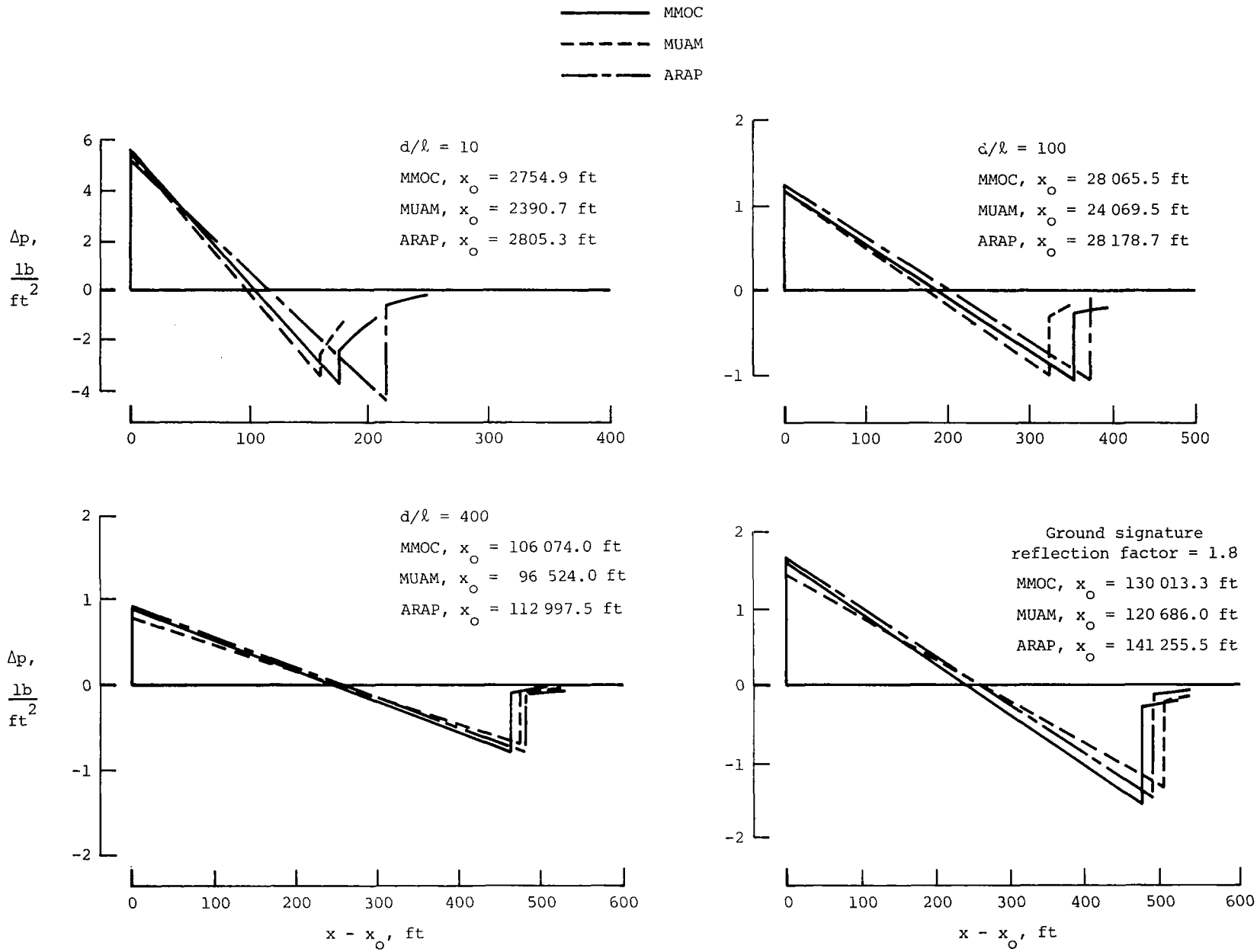

Figure 7.- Concluded.

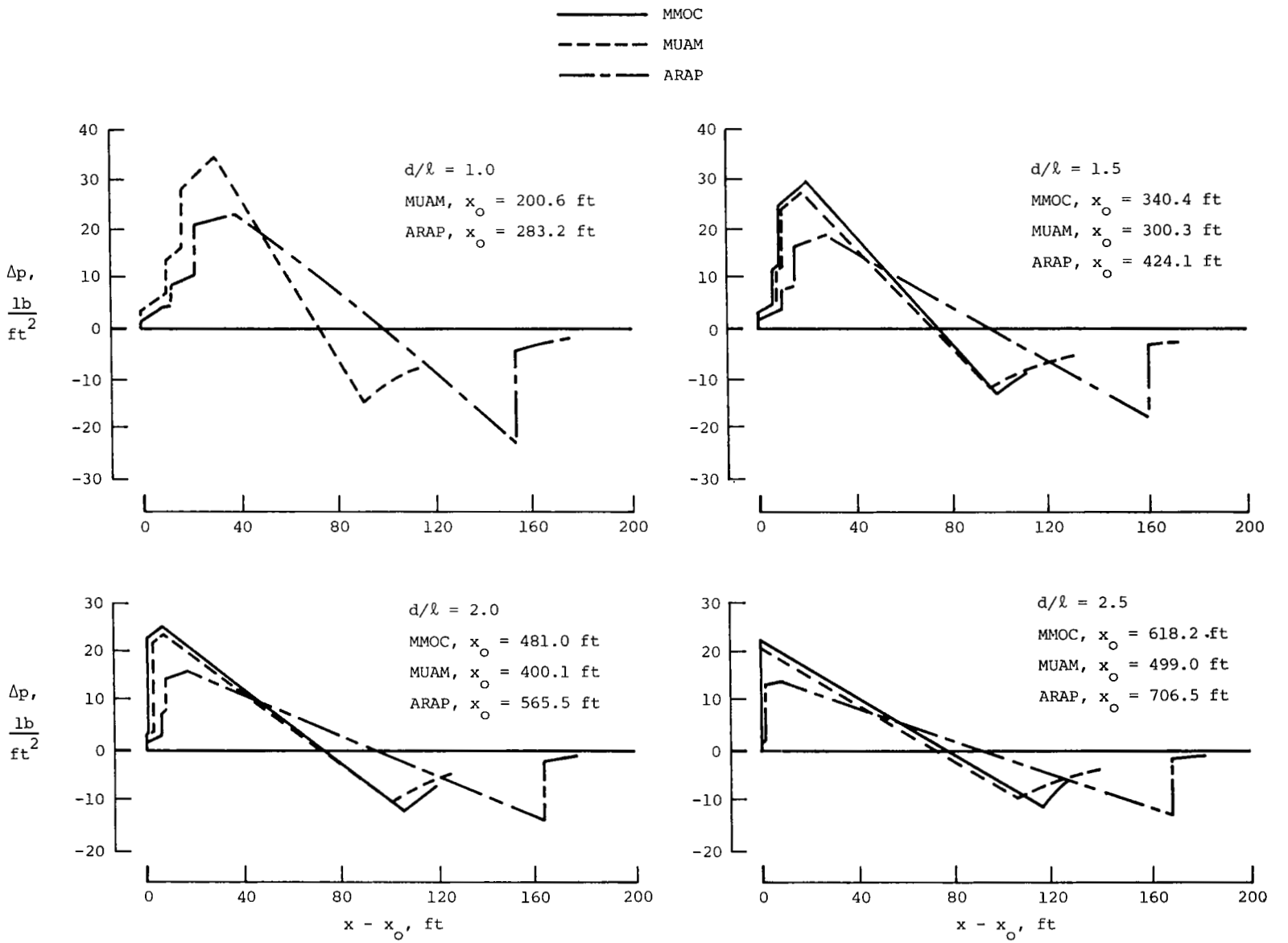

Figure 8.- Comparison of pressure signatures at M = 3.00 and α = 7°. Body of revolution as shown in figure 5; ℓ = 100 ft; alt = 50 000 ft.

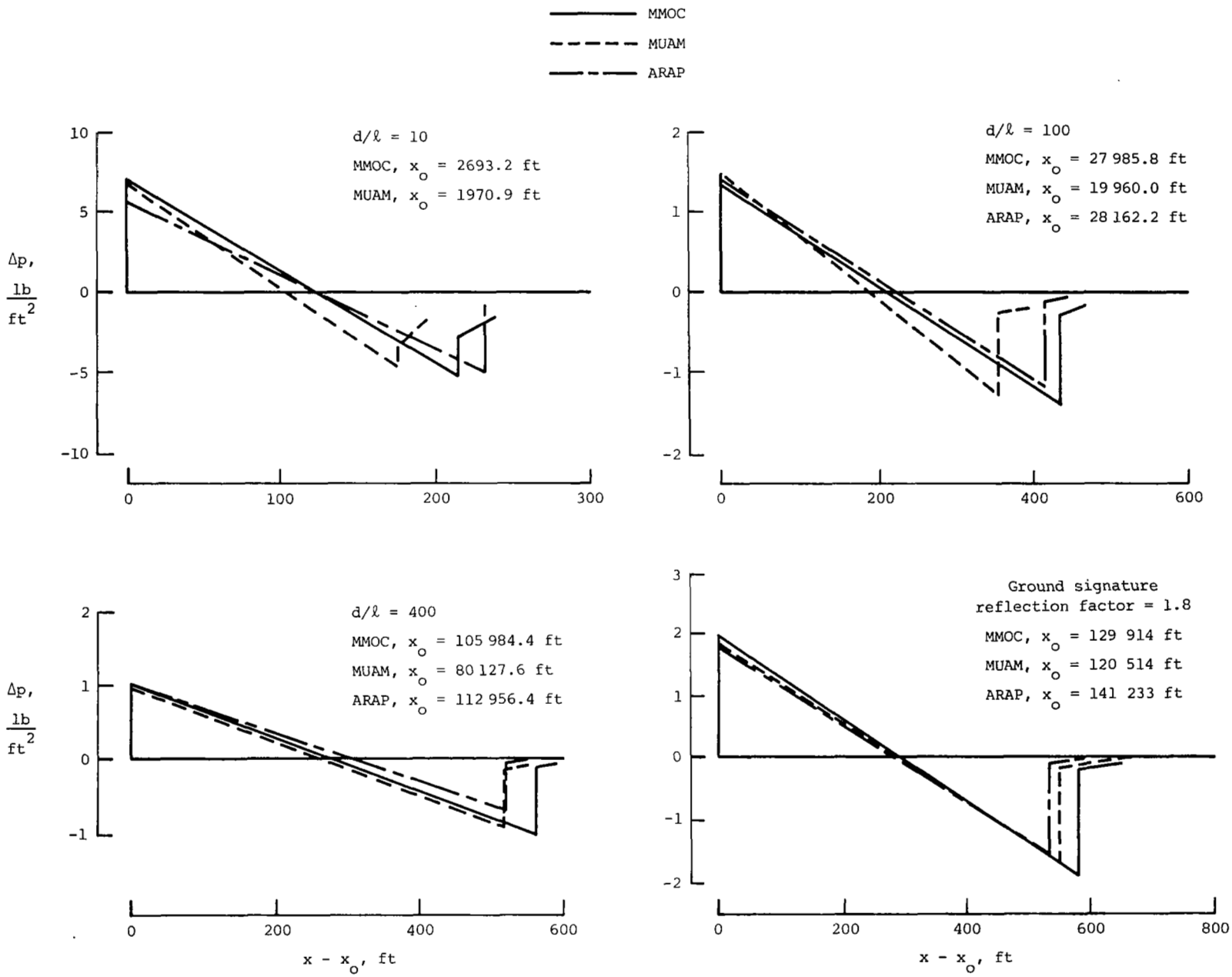

Figure 8.- Concluded.

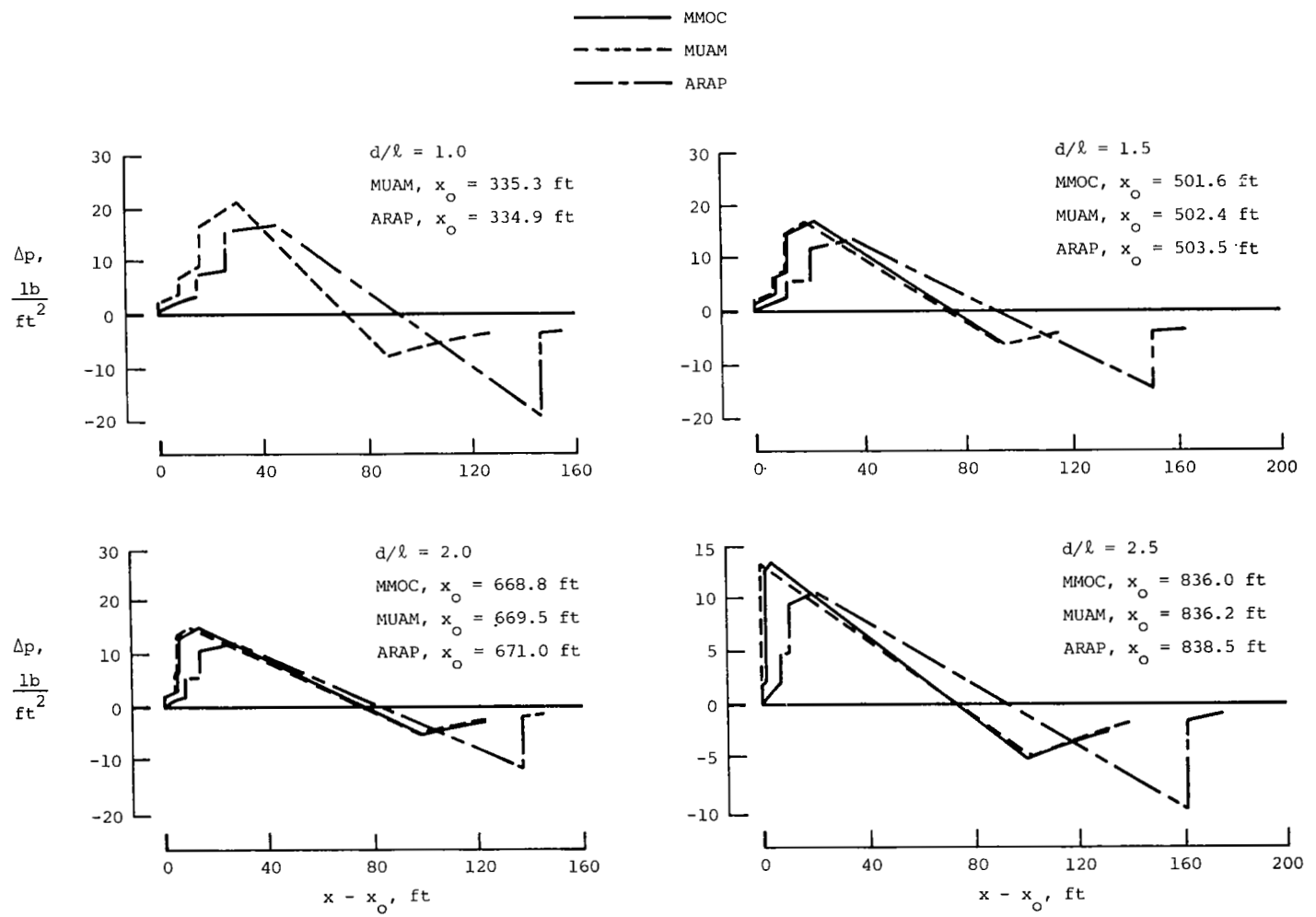

Figure 9.- Comparison of pressure signatures at M = 3.50 and $\alpha = 0°$. Body of revolution as shown in figure 5; ℓ = 100 ft; alt = 50 000 ft.

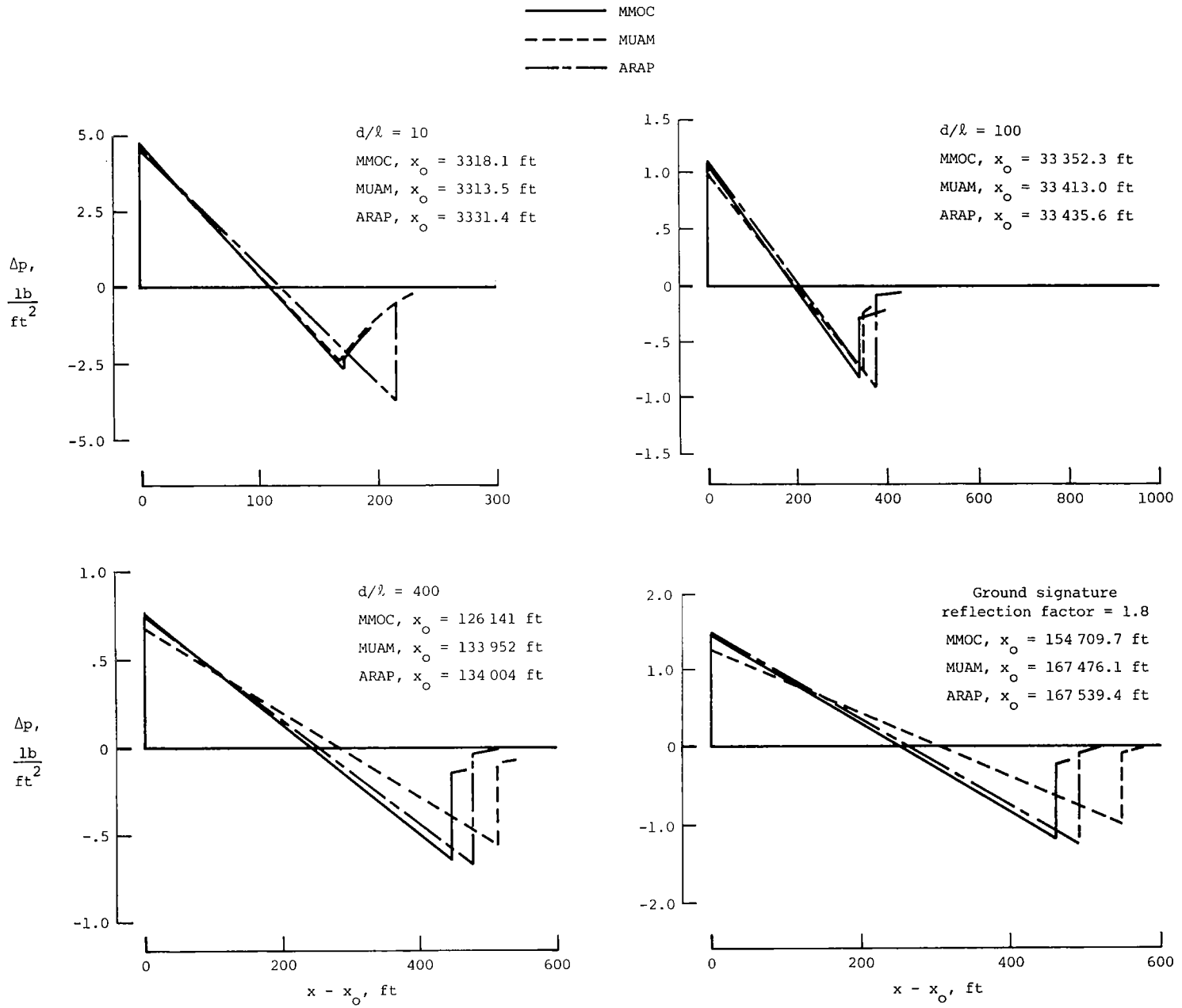

Figure 9.- Concluded.

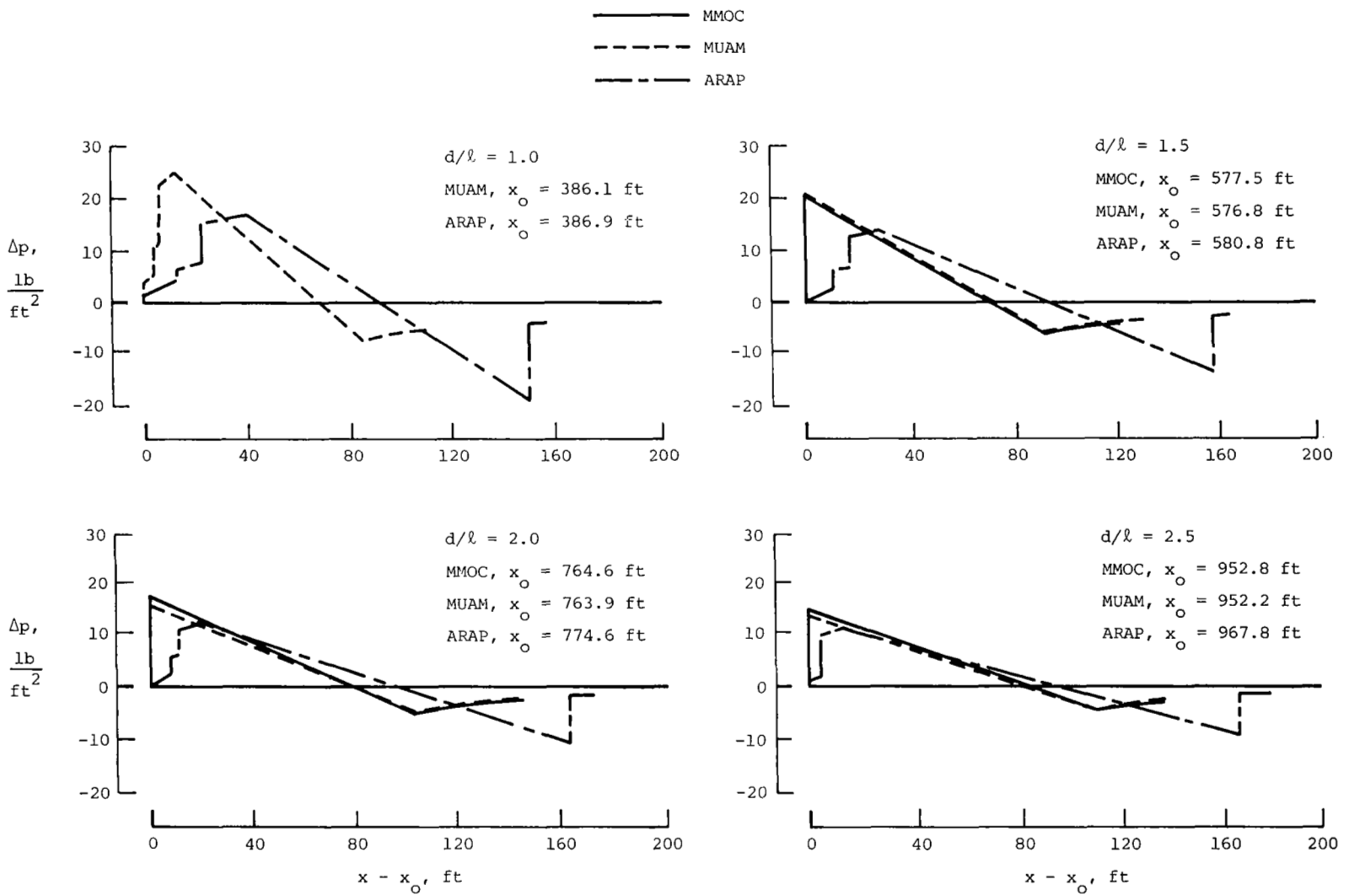

Figure 10.- Comparison of pressure signatures at M = 4.00 and $\alpha = 0°$. Body of revolution as shown in figure 5; ℓ = 100 ft; alt = 50 000 ft.

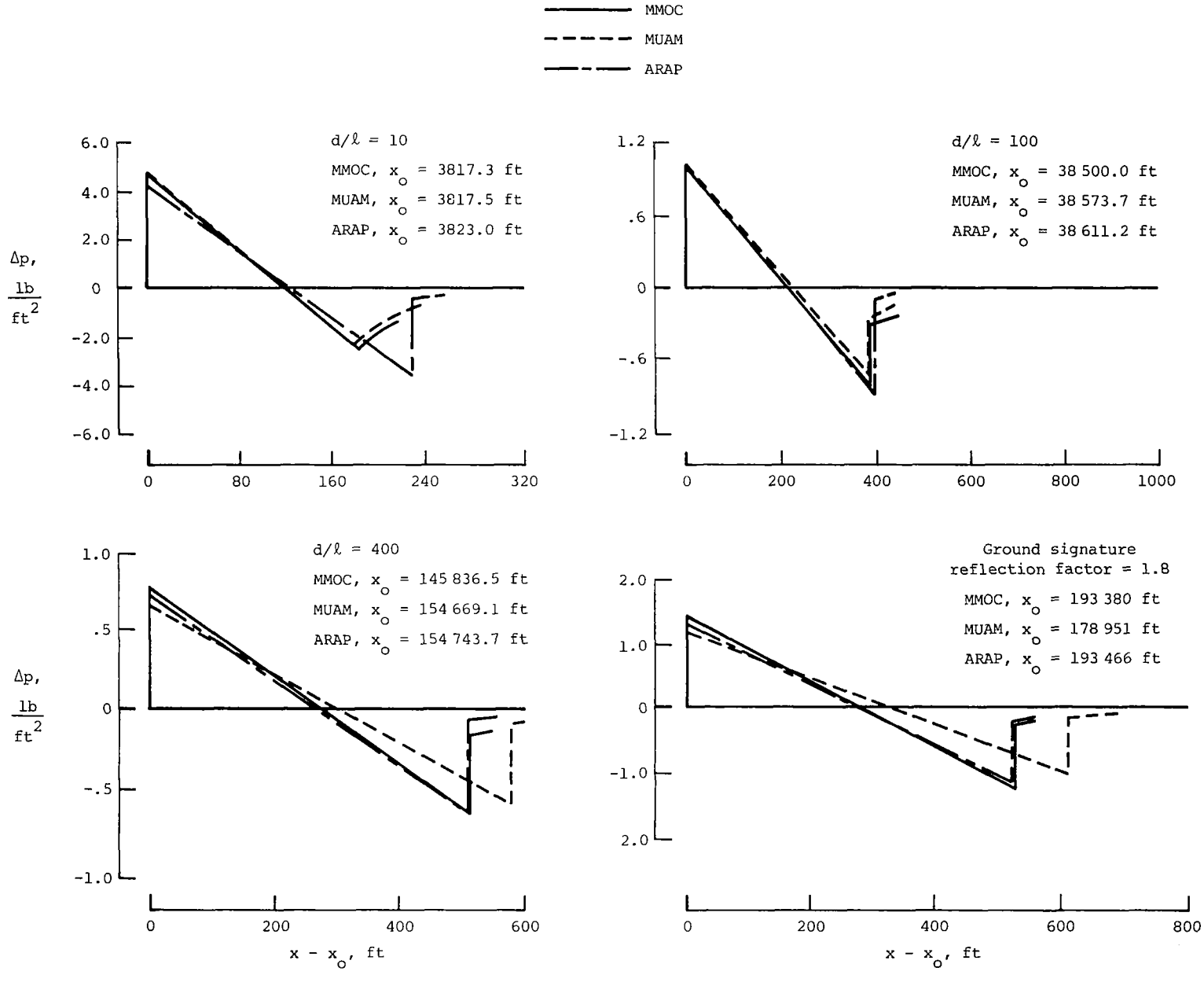

Figure 10.- Concluded.

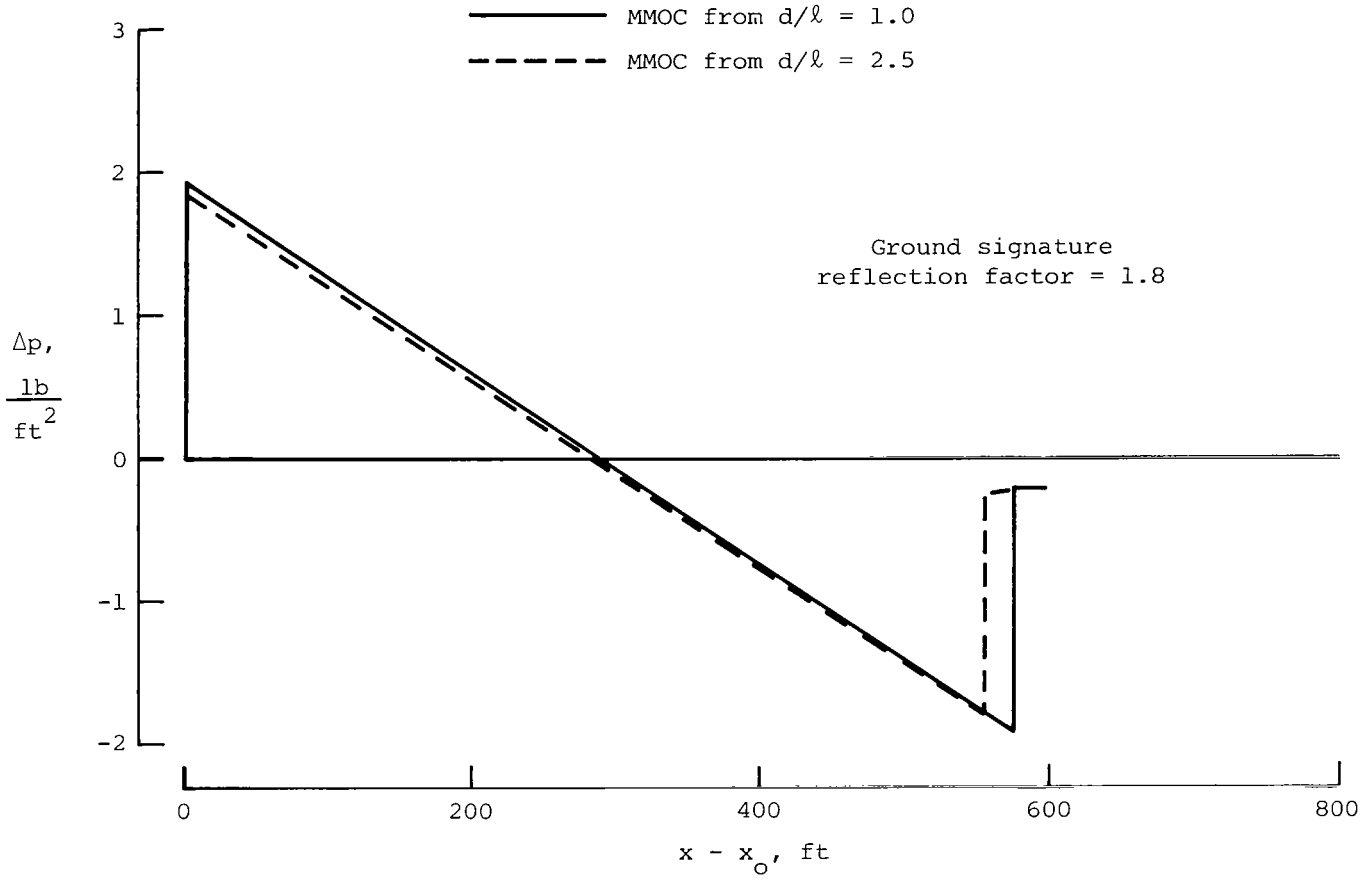

Figure 11.- Comparison of extrapolations from two radial distances. Body of revolution as shown in figure 5; M = 3.00; α = 7°; ℓ = 100 ft; alt = 50 000 ft.

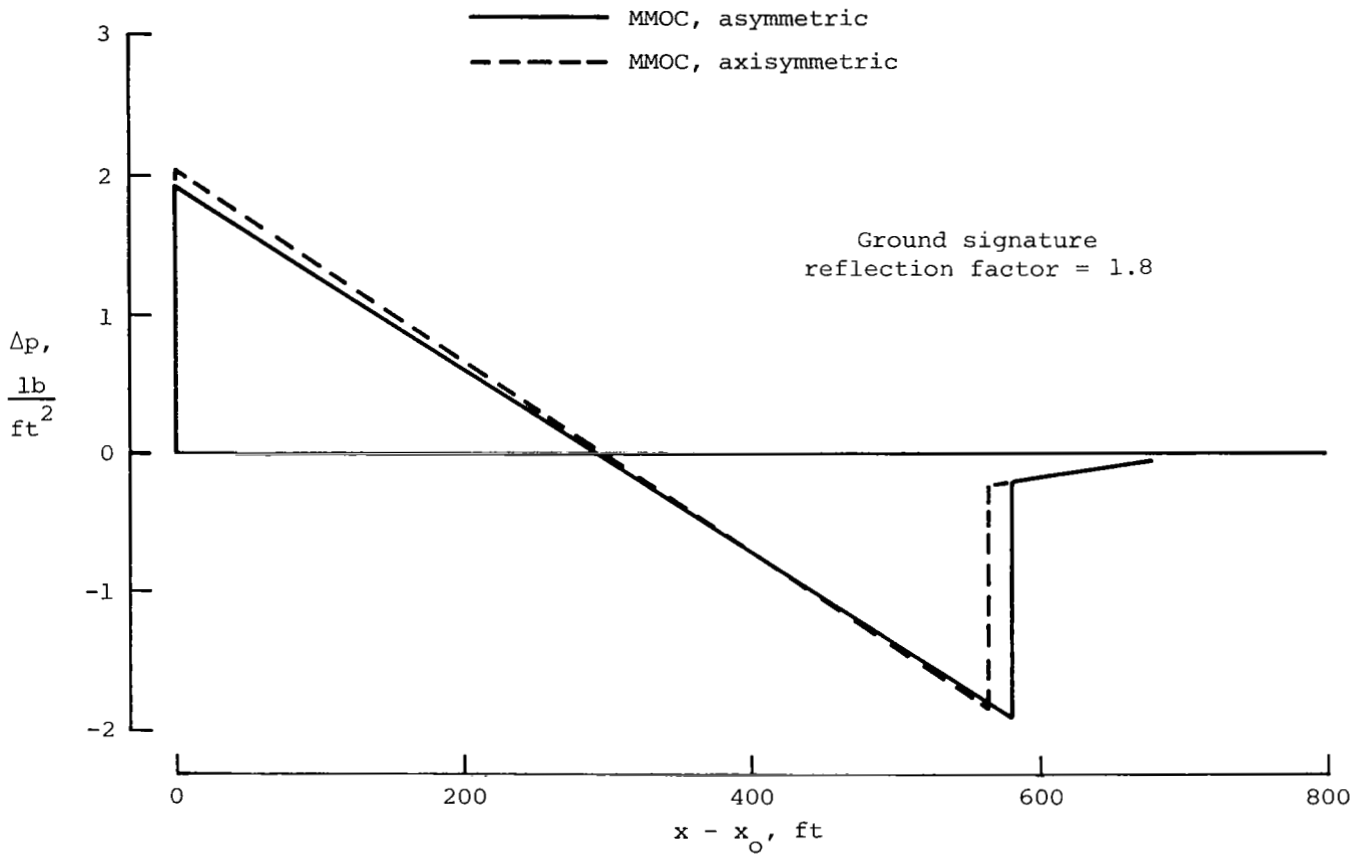

Figure 12.- Comparison of extrapolations with and without asymmetric effects. Body of revolution as shown in figure 5; M = 3.00; α = 7°; ℓ = 100 ft; alt = 50 000 ft.

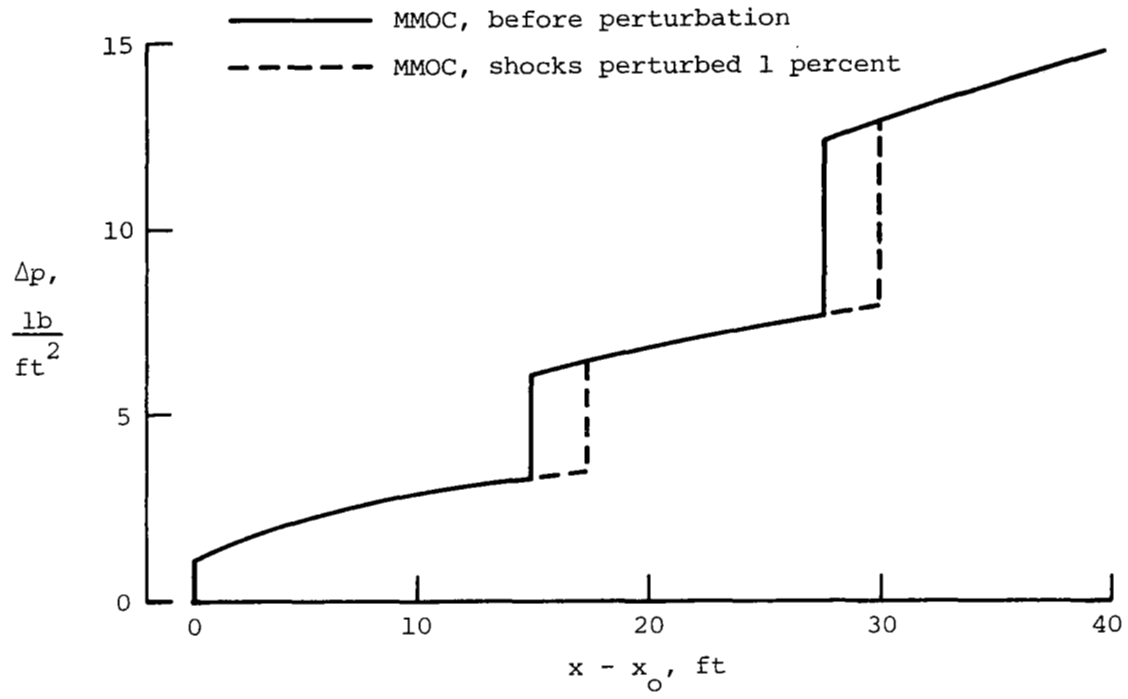

(a) Signatures at $d/\ell = 1.0$.

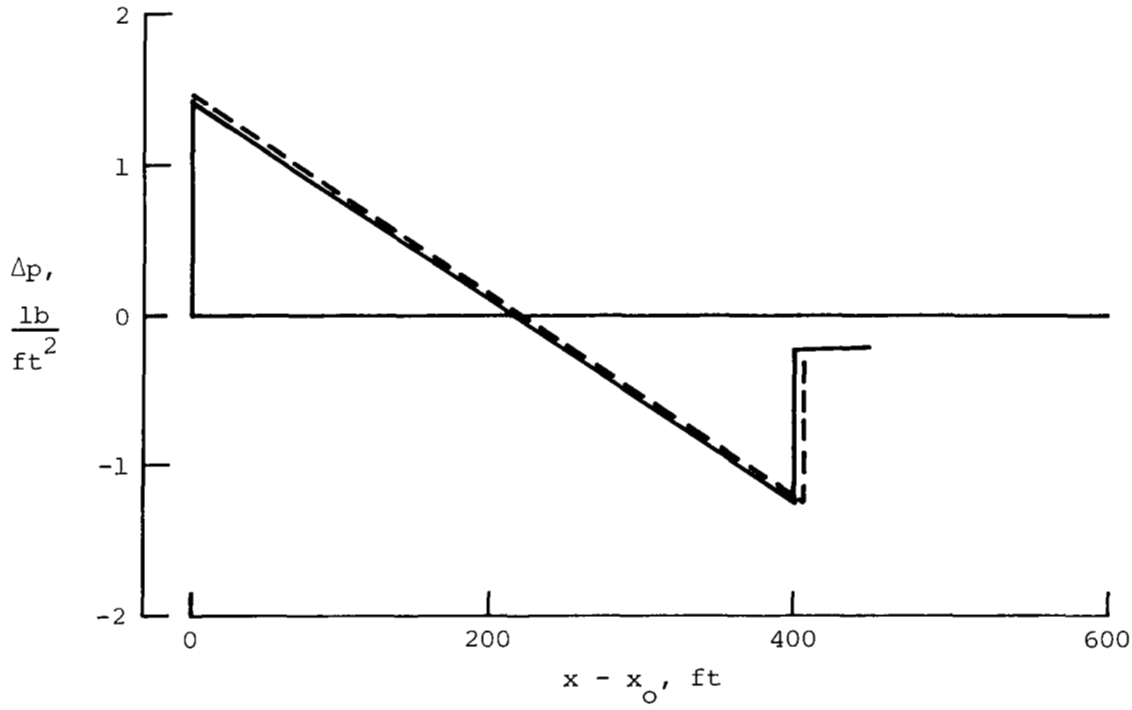

(b) Ground signatures.

Figure 13.- Comparison of pressure signatures when location of shock is perturbed. Body of revolution as shown in figure 5; M = 3.00; $\alpha = 0°$; $\ell = 100$ ft; alt = 50 000 ft.

1. Report No.	2. Government Accession No.	3. Recipient's Catalog No.
NASA TP-2214		

4. Title and Subtitle	5. Report Date
AN ANALYSIS OF SHOCK COALESCENCE INCLUDING THREE-DIMENSIONAL EFFECTS WITH APPLICATION TO SONIC BOOM EXTRAPOLATION	January 1984
	6. Performing Organization Code 505-31-23-10

7. Author(s)	8. Performing Organization Report No.
Christine M. Darden	L-15660
	10. Work Unit No.

9. Performing Organization Name and Address	11. Contract or Grant No.
NASA Langley Research Center Hampton, VA 23665	
	13. Type of Report and Period Covered Technical Paper

12. Sponsoring Agency Name and Address	14. Sponsoring Agency Code
National Aeronautics and Space Administration Washington, DC 20546	

15. Supplementary Notes

16. Abstract

A method for analyzing shock coalescence which includes three-dimensional effects is developed. The method is based on an extension of the axisymmetric solution, with asymmetric effects introduced through an additional set of governing equations, derived by taking the second circumferential derivative of the standard shock equations in the plane of symmetry. The coalescence method is consistent with and has been combined with a nonlinear sonic boom extrapolation program which is based on the method of characteristics. The extrapolation program, originally unable to handle shock coalescence, is now able to extrapolate pressure signatures which include embedded shocks from an initial data line in the plane of symmetry at approximately one body length from the axis of the aircraft to the ground. Descriptions of the axisymmetric shock coalescence solution, the asymmetric shock coalescence solution, the method of incorporating these solutions into the extrapolation program, and the methods used to determine spatial derivatives needed in the coalescence solution are included. Results of the method are shown for a body of revolution at a small, positive angle of attack. The body was designed so that embedded shocks would be included in the near-field data.

17. Key Words (Suggested by Author(s))	18. Distribution Statement
Shock coalescence Sonic boom Supersonic flow	Unclassified - Unlimited Subject Category 34

19. Security Classif. (of this report)	20. Security Classif. (of this page)	21. No. of Pages	22. Price
Unclassified	Unclassified	77	A05

For sale by the National Technical Information Service, Springfield, Virginia 22161

NASA-Langley, 1984